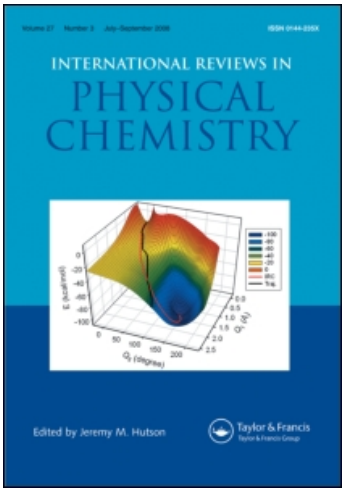

International Reviews in Physical Chemistry
Publication details, including instructions for authors and subscription information:
http://www.informaworld.com/smpp/title~content=t713724383

The halocarbenes: model systems for understanding the spectroscopy, dynamics and chemistry of carbenes

Scott H. Kable[a]; Scott A. Reid[b]; Trevor J. Sears[c]
[a] School of Chemistry, University of Sydney, Sydney, NSW 2006, Australia [b] Department of Chemistry, Marquette University, Milwaukee, WI 53201-1881, USA [c] Department of Chemistry, Brookhaven National Laboratory, Upton, NY 11973, USA

To cite this Article Kable, Scott H. , Reid, Scott A. and Sears, Trevor J.(2009) 'The halocarbenes: model systems for understanding the spectroscopy, dynamics and chemistry of carbenes', International Reviews in Physical Chemistry, 28: 3, 435 — 480
To link to this Article: DOI: 10.1080/01442350903087792
URL: http://dx.doi.org/10.1080/01442350903087792

International Reviews in Physical Chemistry
Vol. 28, No. 3, July–September 2009, 435–480

Taylor & Francis
Taylor & Francis Group

The halocarbenes: model systems for understanding the spectroscopy, dynamics and chemistry of carbenes

Scott H. Kable[a]*, Scott A. Reid[b]* and Trevor J. Sears[c]*

[a]*School of Chemistry, University of Sydney, Sydney, NSW 2006, Australia;*
[b]*Department of Chemistry, Marquette University, Milwaukee, WI 53201-1881, USA;*
[c]*Department of Chemistry, Brookhaven National Laboratory, Upton, NY 11973, USA*

(*Received 3 April 2009; final version received 13 April 2009*)

We review recent studies of the spectroscopy and dynamics of halocarbenes :CXY (X = H, F, Cl, Br, I; Y = F, Cl, Br, I), which are set forth as model systems for understanding the spectroscopy, photochemistry and photophysics of carbenes, and benchmarks for comparing experiment and theory concerning carbene singlet–triplet gaps and spin–orbit coupling from the limit of mixing of isolated rovibronic levels to energy perturbations involving entire vibronic levels. Following a historical overview of halocarbene chemistry, which spans more than 50 years, we discuss experimental methods for generating and spectroscopically detecting these elusive species. Subsequent sections focus on: (a) the spectroscopy of the halocarbenes, where a variety of non-adiabatic interactions are operative, (b) the singlet–triplet gap in the halocarbenes, where experimental methods for measuring this quantity are outlined and their results are compared with benchmark theoretical calculations and (c) the photochemistry and photodissociation dynamics of the halocarbenes, which emphasises recent observations of the hitherto unobserved quasilinear *B* state.

Keywords: carbenes; halocarbenes; laser spectroscopy; singlet-triplet gap; photochemistry; Renner-Teller effect; spin-orbit coupling; axis-tilting

Contents

*Corresponding authors. Emails: s.kable@chem.usyd.edu.au; scott.reid@mu.edu; sears@bnl.gov

ISSN 0144–235X print/ISSN 1366–591X online

DOI: 10.1080/01442350903087792
http://www.informaworld.com

1. Introduction

Beginning from experiments of half a century ago which showed the lack of selectivity in the insertion reactions of methylene (:CH_2) [1,2], the reactivity of carbenes has been extensively studied, and continues to be an active area of research. Carbenes hold a special place in the annals of reactive intermediate chemistry, as evidenced in a recent compilation that devoted five chapters to the topic of carbene structure and reactivity [3]. The interest in carbenes stems in part from the electronic structure of the two lowest electronic states, denoted by S_0 and T_1 for carbenes with singlet ground states (Figure 1). The nonbonding electrons can be spin-paired in the HOMO, an in-plane sp^2-hybridised orbital, giving rise to the singlet, or unpaired with one electron promoted to the LUMO, an out-of-plane carbon centred p_x orbital, producing the triplet. Given the significant differences in reactivity expected for these states, several important questions arise. Which of the

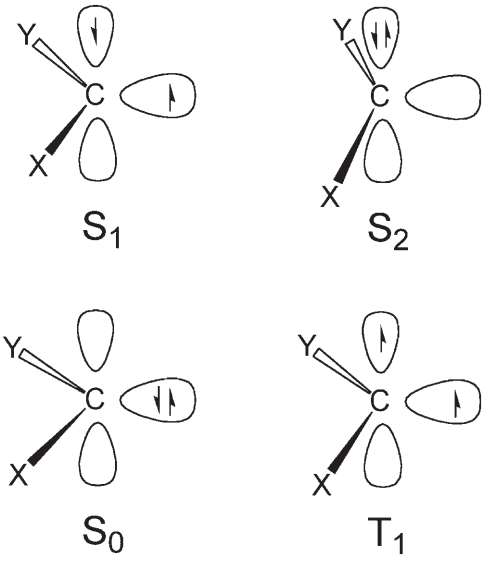

Figure 1. Schematic representations of the electronic structure of the three lowest singlet (S_0, S_1 and S_2) and lowest triplet (T_1) state of a triatomic carbene :CXY.

configurations (singlet *vs*. triplet) is lower in energy? What is the gap between them, and how is it controlled by substituent-dependent steric and electronic affects? The answers to these questions are not obvious, and have stimulated much research in the field.

Coincident with the development of new experimental and theoretical methods over the past several decades, our understanding of the spectroscopy, structure and reactivity of carbenes has blossomed. Indeed, the synergy between experiment and theory, which is a hallmark of modern chemistry, permeates the history of carbene chemistry. For example, the particular question of the equilibrium structure of methylene (linear or bent?) represented one of the first real triumphs of *ab initio* theory, and an illustrative example of theory leading experiment. The story, as beautifully recapped in a review by Schaefer [4], begins with one of the earliest *ab initio* calculations on a polyatomic molecule [5], which predicted a bent equilibrium structure for the triplet ground state of methylene. This finding was later called into question, first by an experimental analysis of the methylene absorption spectrum by Herzberg [6] and subsequently by the empirical treatment of Jordan and Longuet-Higgins [7], both of which suggested a linear equilibrium structure for the triplet. Semi-empirical (CNDO) [8] and *ab initio* valence bond studies [9] followed, favouring the bent structure; however, these authors were hesitant to contradict the seemingly firm experimental evidence for a linear geometry. A subsequent *ab initio* study from Schaefer and co-workers using then novel Configuration Interaction (CI) methods also found a bent equilibrium geometry for the triplet [10]. Around the same time, electron spin resonance (ESR) experiments from Benheim [11,12] and Wasserman [13] indicated that, indeed, the triplet ground state of methylene was bent, and the equilibrium bond angle derived from the ESR data was in excellent agreement with the *ab initio* predictions.

The history of halocarbene chemistry is nearly as old as that of carbene chemistry itself, dating back to the experiments of Hine which elucidated the formation of $:CCl_2$ in the

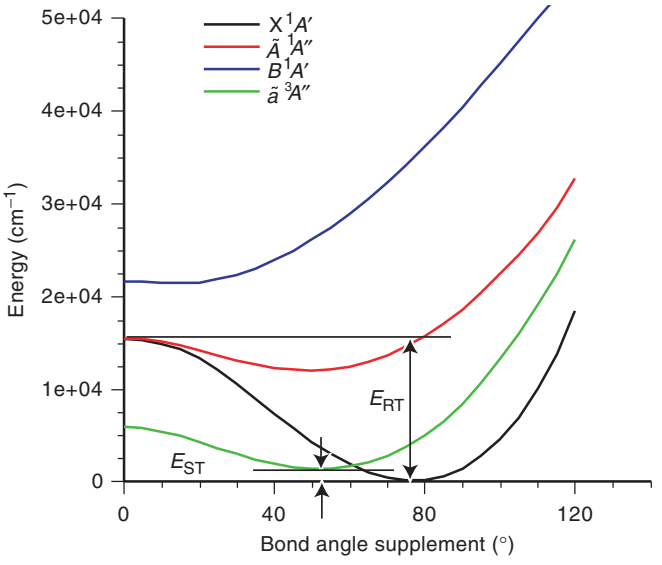

Figure 2. [Colour online] Bending potential curves for the lowest four states of :CHBr from a MRCI/cc-pVTZ calculation [118]. These are typical of the situation for all the halocarbenes, although the relative positions vary according to the particular species. For the purposes of this figure, the HCBr bond lengths are fixed at values appropriate for the $\tilde{A}$ state of the molecule. The arrows indicate the equilibrium triplet–singlet splitting and the RT energy as defined in the present article.

hydrolysis of chloroform [14], and the studies of Doering and Hoffmann which showed that :CCl_2 reacted with olefins to produce cycloalkanes [15,16]. Wescott showed that pyrolytically generated :CCl_2 reacted stereospecifically with *cis*- and *trans*-2-butene when condensed with olefins at low temperature, and suggested a singlet ground state [17]. Indeed, all of the known triatomic halocarbenes have singlet ground states, as the singlet is stabilised by back-donation of nonbonding electron density from the halogen to the unfilled carbon-centred p_x orbital. In reactivity studies, :CCl_2 has proven to be the prototypical electrophilic singlet carbene, undergoing electrophilic insertion into C–H bonds and stereospecific electrophilic addition to alkenes [18,19]. Halocarbenes like :CCl_2 have also proven to be valuable benchmarks for comparing experiment with *ab initio* theory. As we will discuss, *ab initio* theory has certainly led experiment regarding halocarbene singlet–triplet gaps.

From the viewpoint of molecular spectroscopy, which is the emphasis provided in this review, the era of gas-phase halocarbene spectroscopy began in 1950 with reports of the emission and absorption spectrum of :CF_2 [20,21]. Subsequent investigations [22–24] revealed a long vibrational progression in the bending mode, which reflects the large change in bond angle from S_0 to S_1 (Figure 2). These states form a Renner–Teller (RT) pair that is degenerate in the linear configuration (Figure 2), and the RT effect refers to the strong nonadiabatic interaction between these states that is maximal near the barrier to linearity. The large change in bond angle also leads to axis-tilting and the appearance of forbidden sub-bands, which was recognised in the very first rotationally resolved spectra of the halocarbenes [25,26]. Thus, despite their apparent simplicity, the spectroscopy and

dynamics of these molecules are in fact quite complicated. In addition to the RT effect, the low-lying triplet state (T_1) can interact with the RT mixed S_0 and S_1 via spin–orbit interaction, which is particularly important in the heavier members of this series. At higher energies, one can access the quasilinear S_2 state (Figure 2), which lies near or above channels for dissociation via the elimination of a hydrogen halide or simple C–H or C–X bond fission. Despite their known status as products of halocarbon photodecomposition, only very recently have studies of the photochemistry of even the simplest halocarbenes been initiated.

In this review we focus on the triatomic halocarbenes (:CXY; X = H, F, Cl, Br, I; Y = F, Cl, Br, I), which have been extensively studied in our laboratories over the past decade, and aspire to make the case that these are model systems for understanding carbene spectroscopy, singlet–triplet gaps, photochemistry and photophysics. The outline of the review is as follows. Section 2 summarises methods for generating halocarbenes and their spectroscopic interrogation. Section 3 focuses on the complicated spectroscopy of the halocarbenes, emphasising the RT effect and spin–orbit coupling. Section 4 focuses on experimental and theoretical studies of the singlet–triplet gap in halocarbenes, while Section 5 summarises what is currently known regarding the photochemistry of the halocarbenes. We conclude in Section 6 by offering our perspective on future trends in the study of halocarbene spectroscopy and dynamics.

2. Experimental methods

2.1. *Methods for generating halocarbenes*

As with other reactive intermediates, the generation of halocarbenes in quantities sufficient for spectroscopic interrogation can generally be achieved through several routes from an appropriate precursor: pyrolysis, photolysis, and electrical or microwave discharge being the most commonly applied. Essentially all of these methods have been used at some point in our laboratories, depending on the type of experiment, and here we discuss the basics of each.

2.1.1. *Pyrolysis*

The success of pyrolytic methods for carbene production dates back to the 1913, when Staudinger and Engle produced phenylcarbene from the flash vacuum pyrolysis of diphenylketene [27]. For halocarbenes, early studies include that of Blanchard and Le Goff [28], who showed that the thermal decomposition of CCl_4 on hot tungsten surfaces produced $:CCl_2$, and Bevan *et al.* [29], who produced $:CCl_2$ from pyrolysis of CCl_3SiCl_3 at 250°C. Shapiro and Lossing [30] used a similar approach to determine the ionisation potential and heat of formation of $:CCl_2$ by mass spectrometric methods. Skell and Cholod [31] generated $:CCl_2$ under vacuum by the pyrolysis of $CHCl_3$ or CCl_4, at temperatures near 1500°C. From the viewpoint of molecular spectroscopy, an advance came in the mid-1980s with the advent of jet pyrolysis methods, pioneered by Grant [32] and Chen and Colson [33–35], which combined flash pyrolysis with molecular beam methods to produce intense beams of jet-cooled radicals. Several groups immediately implemented this approach to study the electronic spectroscopy of $:CCl_2$. Thus, flash pyrolysis of $(CH_3)_3SiCCl$ at 500°C in a continuous source [36,37], or concerted HCl loss

from $CHCl_3$ pyrolysed at ~1100°C in a pulsed source [38,39], yielded the carbene $:CCl_2$ in good yield. More recently, the microwave spectrum of $:CCl_2$ has been obtained using a pyrolysis source [40].

A new design of the pulsed jet pyrolysis source was reported by one of us (S.H. Kable) [41], who produced $:CF_2$ from pyrolysis of C_2F_4, [42] and :CFBr from pyrolysis of $CHFBr_2$ [43,44]. More recently, the pyrolysis jet technique was used by Dagdigian and co-workers to produce :CFBr [45], :CFCl [45] and $:CCl_2$ [46–48] for studies of their ultraviolet photodissociation dynamics. The advantage of the pyrolysis nozzle lies in the clean generation of reactive intermediates that is possible with judicious choice of precursor. However, vibrational degrees of freedom are not cooled effectively in the jet expansion, resulting in sample vibrational temperatures similar to that of the pyrolytic source. This can be a significant complication for spectroscopic experiments. For example, in the laser-induced fluorescence (LIF) spectrum of jet pyrolysed $:CCl_2$, the origin band is buried in the midst of stronger hot bands originating from vibrationally excited levels in the ground state [36,37]. In our experience the rotational temperatures produced by the pyrolysis source are often higher than which can be achieved using photolytic or discharge techniques.

2.1.2. *Photolysis*

Photolytic methods have been successfully applied to generate halocarbenes, in environments ranging from matrix to solution to the gas phase. The initial success dates back to the early studies of Closs and Coyle, who generated :CHCl from the photolysis of chlorodiazomethane [49], which began a long history of the use of diazo compounds and diazirines as carbene precursors [50–52]. Several years later, Dalby [53] used flash photolysis to examine the kinetics of $:CF_2$ reactions, and flash photolysis of matrix-isolated CF_2N_2 gave the first infrared spectrum of $:CF_2$ [52]. The era of high-resolution gas-phase halocarbene spectroscopy arguably began with the seminal work of Merer and Travis [25,26], who observed the visible absorption spectrum of :CHCl and :CHF from flash photolysis of $HCClBr_2$ and $HCFBr_2$, respectively (Note that the first rotationally resolved spectrum of $:CF_2$ was obtained in that same year [54].). The mechanism of halocarbene formation in this case presumably involves halogen loss to form a hot halomethyl radical, which can form the carbene from direct unimolecular decay, or following absorption of a second photon. Soon after, Jacox and Milligan [55] reported the production of :CHF from vacuum-ultraviolet photolysis of CH_3F in an inert gas matrix. As the parent halocarbons typically absorb deep in the ultraviolet, the use of photolytic methods has been greatly augmented by the development of ultraviolet laser sources such as the excimer laser, and flash laser photolysis continues to be widely employed [56].

In combining the photolysis with molecular beam methods, one typically photolyzes the precursor just at the nozzle exit, which allows for efficient cooling of the generated fragments and minimises bimolecular chemistry. The internal energy content of the fragment carbene can be minimised by judicious choice of precursor and photolysis wavelength. Thus, one of us (S.H. Kable) has used this approach to generate :CFCl from the photolysis of $CFClBr_2$ at 239.5 nm [57].

In addition to UV photolysis, infrared laser photolysis by multi-photon dissociation (IRMPD) has also been reported [58–61]. Thus, IRMPD of CF_2HCl not only produces $:CF_2$ as the dominant product, but also :CHCl, :CHF and :CFCl [58]. One of the earliest

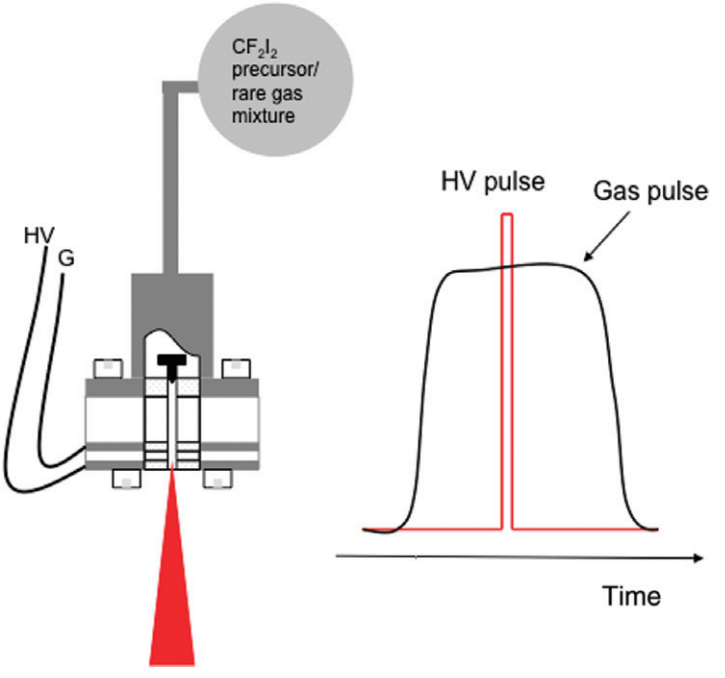

Figure 3. [Colour online] Typical design for a pulsed discharge carbene source. For fluorescence experiments, the use of a short (10–50 μs) high-voltage pulse within the gas pulse minimises interference from the discharge glow.

gas-phase LIF studies of :CHF [61], and the earliest kinetics studies of its gas-phase reactions [60], utilised this method of production.

2.1.3. *Discharge methods*

In recent years, the pulsed jet discharge method has been extensively applied to examine the spectroscopy and dynamics of the halocarbenes. In this method, illustrated in Figure 3, a dilute (*ca* 1%) mixture of a stable carbene precursor in a rare gas (typically He or Ar) is subjected to a high-voltage pulse. Carbenes are formed by direct electron impact on the precursor or by reaction of the precursor with metastable rare gas atoms produced in the discharge; the latter mechanism is probably more important. Although fragmentation in the discharge source is less selective than pyrolysis or photolysis, and the fragmentation efficiency is typically smaller, it works well when matched with a selective and sensitive detection technique like LIF. In this case, a short high-voltage pulse can be used to help discriminate against the discharge glow (Figure 3). Moreover, by working at voltages close to threshold and minimising the discharge current, one can minimise secondary fragmentation. The use of discharge methods for carbene generation date back to early experiments of Steudel [62], and the combination of discharge and supersonic jet methods was, to our knowledge, first reported by Dobrynin *et al.*, in 1979 [63]. The earliest recorded implementation in molecular spectroscopy was, not surprisingly, to produce intense beams

of :CF_2 [32]. In that study, Grant and co-workers noted that the discharge nozzle produced a carbene number density about 1 order of magnitude less than a similarly configured pyrolysis nozzle.

Some of the first applications of the pulsed discharge nozzle to carbene spectroscopy were carried out by Schlachta *et al*. [64–66] who reported LIF spectra of jet-cooled :CFCl [65] and :CBrCl [65]. The same group later reported a novel mating of the discharge nozzle with matrix isolation [67], which led to the first tentative spectroscopic observation of an iodocarbene, :CFI. The first Doppler-limited high-resolution electronic spectrum of a halocarbene, that of :CHCl reported by Kakimoto *et al*. [68] was obtained using a reactive discharge method, where F atoms produced in a discharge of CF_4 reacted with CH_3Cl. As will be clear in the following, recent gas-phase studies of the halocarbenes have made extensive use of the discharge nozzle and supersonic expansion method.

2.2. *Methods for detecting halocarbenes*

2.2.1. *Absorption methods*

As mentioned above, the era of gas-phase halocarbene spectroscopy really began with emission and flash photolysis absorption spectroscopy of :CF_2 [20,21], and the first high-resolution absorption spectra of :CF_2, :CHCl and :CHF were reported in 1966 using flash photolysis [25,26,54]. Absorption spectroscopy has continued to be an effective method for halocarbene spectroscopy, with many recent advances by made one of us (T.J. Sears). Thus, a time-resolved frequency modulation technique of exquisite sensitivity was developed [69], and applied to the near-infrared spectroscopy of the halocarbenes :CHCl and :CHBr [70–79]. The use of this method in the study of the singlet–triplet gap and spin–orbit mixing in these species is outlined in Section 4 of this article.

2.2.2. *Laser-induced fluorescence*

Fluorescence-based methods have been very important in halocarbene spectroscopy [42,43,57,61,68,80–113]. LIF is a very sensitive, selective and background-free technique for fluorescing states, and, since the S_0–S_1 origins of all the halocarbenes nearly lie in the near-infrared to near-ultraviolet region, typically below the energetic threshold of any dissociation channel, the fluorescence quantum yields are usually high. The exception is for states lying above the RT intersection, where strong non-adiabatic interactions lead to extensive mixing of sub-bands with $K>0$ and a pronounced lifetime lengthening [86,91,104]. However, in this case fluorescence lifetime measurements can provide a sensitive diagnostic of the RT interactions.

Due to the large change in bond angle in the S_0–S_1 transition of the halocarbenes, the Franck–Condon factors are highly non-diagonal in the bending mode, producing a large red-shift in fluorescence, as shown in Figure 4. This facilitates LIF detection by affording good discrimination against scattered laser light. Additionally, LIF is well matched with pulsed molecular beam methods, which have been widely used for halocarbene generation, as described earlier. Finally, fluorescence emission spectra have been particularly important in experimental studies of halocarbene singlet–triplet gaps, as we outline in Section 4. Figure 4 displays a schematic representation of a typical

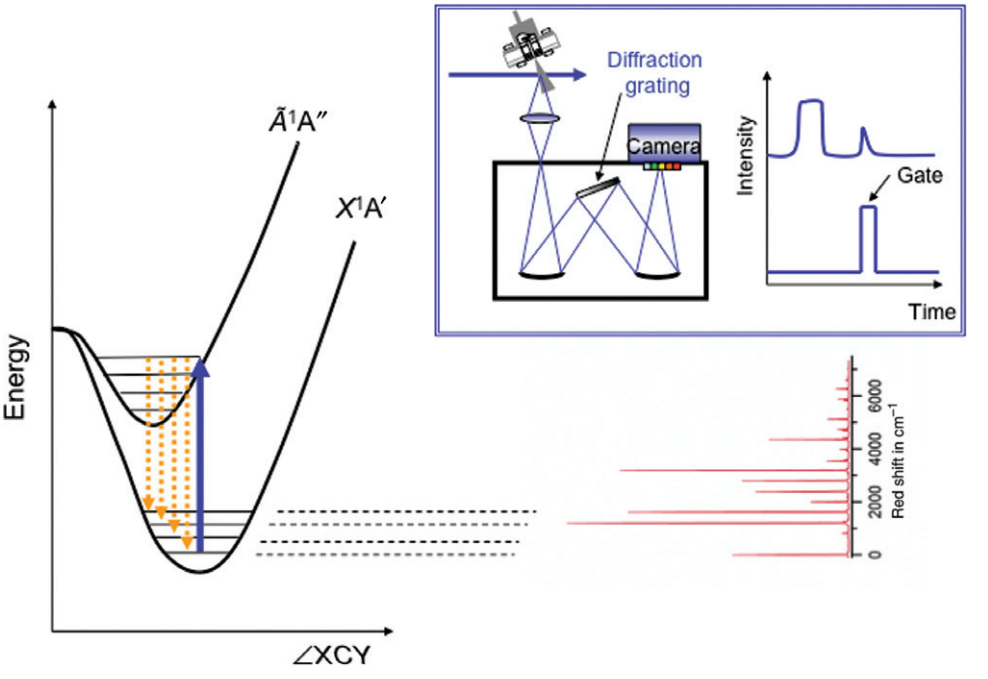

Figure 4. [Colour online] Illustration of the SVL emission technique applied to probe the singlet–triplet gap and spin–orbit perturbations between the lowest singlet and triplet states in halocarbenes. Modern spectrographs are usually equipped with a gated, intensified CCD detector as shown in the figure.

Single Vibronic Level (SVL) emission experiment using a pulsed discharge source and charge-coupled device (CCD) equipped spectrograph.

2.2.3. *Photoionisation and photoelectron spectroscopy*

Due to their relatively high ionisation potentials (IPs), there have been relatively few reports of the direct detection of halocarbenes by photoionisation methods. Hudgens and co-workers reported 2 + 1 Resonantly Enhanced MultiPhoton Ionisation spectroscopy (REMPI) of :CHF between 304 and 325 nm through a high-lying 3p Rydberg state [114], Recently, Fischer and co-workers reported ultrafast time-resolved photoionisation and photoelectron imaging measurements of pyrolytically generated chlorophenylcarbene excited at 265 nm into the $3^1A'$ state [115]. The application of time-resolved photoionisation and photoelectron methods is an exciting development in the study of carbene spectroscopy and dynamics. In Section 4 we describe the use of negative ion photoelectron spectroscopy (PES) to probe the singlet–triplet gaps of the halocarbenes.

3. The complicated spectroscopy of the halocarbenes

3.1. *General features of halocarbene spectroscopy*

Systematic experimental studies of the electronic spectroscopy of triatomic halocarbenes began in the 1960s at the National Research Council of Canada. Shortly after the classic

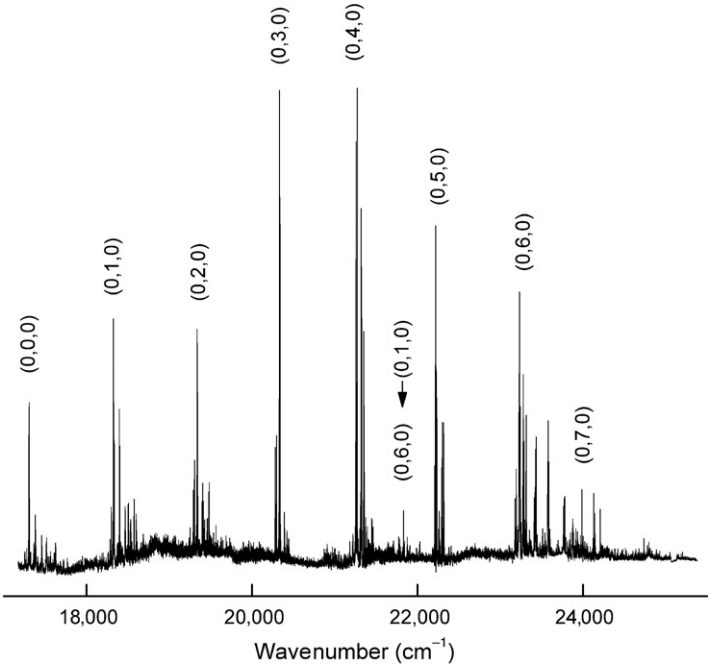

Figure 5. Survey spectrum of the $\tilde{A}A'' - \tilde{A}A'$ band system of :CHF recorded by LIF. Adapted from reference [80]. The spectrum illustrates the extended bending progression typical of the halocarbene singlet band systems. The rotational structure changes from one dominated by strong ${}^{R}Q_0(J)$ band heads at the longer wavelength end to one where the ${}^{P}Q_1(J)$ and ${}^{Q}Q_0(J)$ band heads are strongest above (040). This is symptomatic of the onset of RT coupling as the upper state energy approaches that of the linear configuration. Sequence band structure in ν_3 complicates the longer wavelength bands and :CFBr band interference is visible between (060) and (070).

report of the spectroscopic analysis of the singlet absorption spectrum of :CH_2 by Herzberg and Johns [116], Merer and Travis reported the observation of the analogous spectra of :CHCl [25] and :CHF [26]. Common to all these observed spectra is an extended Franck–Condon progression in the bending vibrational mode which occurs because the ground $\tilde{X}\ {}^1A'$ state of the halocarbenes is quite strongly bent, while the excited $\tilde{A}\ {}^1A''$ state is much closer to linearity. An example from more recent work [80] is shown in Figure 5. Simple halocarbenes possess 12 valence electrons and Walsh's rules [117] qualitatively predict the observations. The lowest singlet states of the molecule derive from a $\ldots(\pi)^4(\pi^*)^2$ ($\tilde{X}\ {}^1\Delta$) configuration at linearity leading to a ground $\ldots(a'')^2(a')^2(a')^2$ ($\tilde{X}\ {}^1A'$) state and an excited $\ldots(a'')^2(a')^2(a')(a'')$ ($\tilde{A}\ {}^1A''$) state as the molecule bends. The $\ldots(\pi)^4(\pi^*)^2$ configuration also results in a low-lying (bent) ${}^3A''$ state whose energy is expected to lie near to the ground state. In :CH_2, this is the ground state of the molecule, but in all halomethylenes it lies above the lowest singlet state in energy. The early observations of :CHCl and :CHF contained no direct information on the relative energy of the triplet and singlet states although it was speculated [25,26] that observed perturbations in $K_a = 0$ levels in the spectra were possibly due to spin–orbit mixing of background triplet state levels. Determination of the exact relative positions of the triplet and singlet states of the

halomethylenes has been a goal of much of the published work and this is considered in detail in the following section.

Modern calculations of the electronic state surfaces of these species have resulted in near quantitative pictures of the relative state energies and their properties. Figure 2 shows an example taken from the work of Hall *et al.* [118] on :CHBr. The degeneracy of the $\tilde{X}$ and $\tilde{A}$ singlet states at linearity and the relative position of the low-lying triplet state are clear. Note that the shape of the bending potentials for the triplet and first excited singlet states are similar because they derive from the same orbital configuration. Also shown in the figure is the calculated position of the second excited singlet state. Transitions to the analogous state of :CH_2 ($\tilde{c}^1A_1$) were first reported by Herzberg and Johns [116], but they were only recently explained and the state was experimentally characterised [119]. For the halocarbenes the state has only been observed in :CHF [103] and :CHCl, where, like :CH_2, higher vibrational levels in the state exhibit predissociation. Future work will no doubt focus on the detection of the analogous vibronic levels in the other halocarbenes as the spectroscopic measurements of the predissociation regions can lead to precise estimates of the bond dissociation energy for the molecule.

The electronic degeneracy in the linear configuration of the singlet results in a classic breakdown of the Born–Oppenheimer separation of electronic and nuclear motion first described theoretically by Renner [120] in 1934 and now known as the RT effect. Classically, we can understand how this arises: as the molecule bends, the nuclear charge distribution is no longer cylindrically symmetric and therefore breaks the Π-orbital degeneracy. Triatomic molecular spectroscopy has driven the development of theory describing the resulting vibronic and ro-vibronic energy levels that result. Early work is described in Herzberg's book [121] and notable advances in the theory have been made by Jungen and Merer [122,123], Brown and Jorgensen [124], Duxbury and co-workers [125–127] and Bunker and Jensen [128]. The application of an adiabatic theory in hyperspherical coordinates [129] for HCBr was described recently by one of us.

The spectroscopy of singlet methylene and its halogenated derivatives have provided a rich testing ground for these models and aspects of the observations are discussed below. Here, some general features of the spectroscopic consequences of the RT effect in these molecules are described. The separation of the two lowest singlet states in the simple carbenes is a direct result of the RT effect. As a consequence, we cannot make the usual Born–Oppenheimer approximation that vibrational energy levels, in particular bending vibrational levels, can be uniquely associated with one or the other electronic surface. In fact, the vibronic wavefunctions for levels with $K_a = (\Lambda + l) \geq 1$, where K_a (in the following, we will use K for K_a throughout) is the projection of J on the a-inertial (linear molecule) axis and Λ and l are the electronic orbital and nuclear vibrational angular momenta on this axis, contain both $\tilde{X}$ and $\tilde{A}$ state character because the RT Hamiltonian couples the $\pm\Lambda$ components of the degenerate electronic state [122]. The exception is for levels with $K = 0$ where the coupling between the electronic components vanishes by symmetry.

These observations qualitatively explain another feature of the overall appearance of the singlet electronic band systems of the halocarbenes. Figure 5 shows the typical progression in the bending vibration that is seen. Near and above the barrier to linearity, the strongest sub-bands are practically always those terminating in $K' = 0$. These levels are the ones whose electronic wavefunctions are unaffected by vibronic (i.e. RT) coupling.

All others possess mixed character and the spectroscopic intensity is shared among all the perturbing levels, resulting in weaker sub-bands. The effect is particularly strong if the excited state level is above the barrier to linearity, as the RT coupling matrix elements can then become very large. Higher K sub-bands will still be discernable in the vibronic bands well below the barrier, as shown in Figure 5 [113]. In this case the barrier to linearity lies some 6600 cm^{-1} above the electronic origin [91,98]. Note that in Figure 5 only sub-bands originating from $K'' = 0,1,2$ are observed even well below the barrier because the sample is jet-cooled.

3.2. *The RT effect*

3.2.1. *:CHF*

Merer and Travis [26] reported the first rotational analysis of the singlet band system soon followed by an infrared matrix isolation spectroscopic study by Jacox and Milligan [130]. Laser spectroscopic studies followed during the next 20 years. The Hirota group in particular published a number of high-resolution studies of individual bands [81–83,131] including several measurements of magnetic field effects in Doppler, and even sub-Doppler [81], resolved spectra which established the Zeeman effect in the origin band of the spectrum that is primarily due to orbital angular momentum resulting from the RT mixing of ground state vibrational levels. Isolated perturbations due to sporadic triplet-level mixing were found, but information on the identity of the perturbing triplet state level was not obtainable. Finally, an optical–optical double resonance (OODR) study [132] established the positions of some additional excited vibrational levels of the ground $\tilde{X}^1A'$ involving the bending and CF stretching modes. Surprisingly in retrospect, there was little additional work published on the overall structure of the band system although the measurement of :CHF spectra in chemiluminescence [133] and LIF following IR multiphoton dissociation [61] and chemical reaction [113] were reported though the 1980s.

A renewed surge of interest in the spectroscopy of the halocarbenes began in the following decade. Irikura *et al.* [114] found a $2+1$ resonance-enhanced multiphoton excitation spectrum via a previously undetected state at 62,154 cm^{-1} assigned to a 3p Rydberg state. As the strength of computational *ab initio* techniques improved, the predictive and analytical power of the results encouraged new experimental investigations and a wealth of new spectroscopic results on :CHF have been reported during the last 10 years. First, new and more precise LIF excitation spectra of the radical in a cold supersonic expansion were reported by Schmidt *et al.* [80] and analysed with the help of new *ab initio* calculations of the properties of the $\tilde{A}$ state surface [109]. The expansion-cooled sample showed low-rotational temperature, making rotational assignments of the bands straightforward, but vibrational cooling was much less complete, and as a result estimates of ground state vibrational frequencies could be made from hot bands. The work considerably extended the vibronic assignments in the $\tilde{A}$ state and all three vibrational frequencies in the $\tilde{A}$ state were assigned. The CH stretching frequency was, however, subsequently updated [110] as better quality data were obtained. Ground state frequencies were measured in a LIF dispersed fluorescence (DF) experiment by Fan *et al.* [92]. For convenience, we have collected together the best available experimental measurements for the vibrational frequencies of all the mono-halomethylenes in their ground and first excited singlet states given in Table 1.

Table 1. Experimentally determined vibrational fundamental frequencies for singlet state monohalocarbenes.[a]

Species	T_{00}	ν_1		ν_2		ν_3	
		$\tilde{X}$	$\tilde{A}$	$\tilde{X}$	$\tilde{A}$	$\tilde{X}$	$\tilde{A}$
:CHF	17,277.731(17) [131]	2642.9(1) [107]	2799.7(12) [110]	1403.204(1) [132]	1021.26 [26]	1192(2) [92]	1269.76(6) [91]
:CDF	17,298.23(2) [98]	1967.4(12) [98]	2105.7(17) [98]	1062.1(1) [98]	786.95(3) [98]	1194.3(17) [92]	1254.05(1) [98]
:$CH^{35}Cl$	12,279.990(10) [73]	2793(4) [97]	2980 [97]	1195.54(1) [70]	872.974(4) [73,74]	811.5962(2) [76]	926.17(1) [70]
:$CD^{35}Cl$[b]	12,913.94(1) [71]	2078(2) [141]	2229.6(1) [102]	893(2) [141]	576 [102]	801(2) [141]	901 [102]
:$CH^{79}Br$	11,972.43(1) [216]	2902(4) [148]	3100 [95]	1117.70(2) [79]	828.790(8) [77]	676.444(3) [79]	762 [95]
:$CH^{81}Br$	11,972.35(1) [216]	2902(4) [148]	3100 [95]	1117.63(2) [79]	828.655(8) [77]	675.276(3) [79]	762 [95]
:$CD^{79}Br$	11,966.27(1) [216]	2078(4) [148]	2350 [96]	833.0(2) [217]	391.12(2) [77,216]	663(2) [202]	738 [96]
:$CD^{81}Br$	11,966.20(1) [216]	2078(4) [148]	2350 [96]	833[c]	390.861(2) [77,216]	663(2) [202]	738 [96]
:CHI	10,500[d]					587(2) [108]	

Notes: [a]Values are quoted in cm^{-1}. Numbers in parenthesis are the estimated measurement errors in units of the least significant figure. The corresponding reference is included in square brackets.
[b]T_{00} for the (010)–(000) band.
[c]Assumed to be the same as $CD^{79}Br$.
[d]Tao *et al.* (unpublished), extrapolated from positions of shorter wavelength bands for :CHI and :CDI.

RT mixing of upper state vibronic levels with $K>0$ is evident in the absorption spectrum as the intensity of rotational sub-bands terminating in $K>0$ and strongly decreases with increasing upper state energy due to the increased dilution of the transition moment among large numbers of vibronic levels. A related observation, nicely demonstrating the effects of the RT vibronic mixing, is an increased fluorescence lifetime with increasing energy reported by Fan *et al.* [86].

Hyperfine and Zeeman effects can provide further insight into the extent of RT and spin–orbit vibronic coupling on a level-by-level basis. One of us [88] detected polarisation quantum beats in the fluorescence of :CHF following excitation of single ro-vibronic levels in the $\tilde{A}\ ^1A''$ state. A Fourier transform of the fluorescence quantum beat signal reveals a simple frequency spectrum characteristic of the hyperfine splitting in the excited state level. The hyperfine splitting in most of the levels derives from the nuclear-spin rotation term in the effective Hamiltonian [134,135], and shows a regular increase in magnitude with increasing upper state energy. Standing apart from the general trend are a small number of severely perturbed vibronic levels that are split and whose hyperfine split rotational structure can only be modelled on the assumption that both RT and spin–orbit mechanisms are operative. Detailed analysis of the data [89] including both Zeeman and hyperfine quantum beats [90] allows one to separate the effects of RT and spin–orbit coupling and identify the positions of specific perturbing triplet state levels. The magnitude of the spin–orbit coupling in :CHF is small compared to that seen in the heavier halomethylenes where perturbations in the ground state pin down the triplet–singlet energy splitting. This aspect of the spectra of these species is discussed in detail in the following sections.

Finally, the observation of predissociation-broadening in rotationally-resolved spectra of the $\tilde{B}^1A'$ state of the molecule by fluorescence dip-detected OODR [103] opens up a new page in the spectroscopy of :CHF. Further study of the predissociating levels and action spectra of the products will permit the determination of the bond dissociation energy of the radical, and the OODR technique permits trivial rotational assignment that will aid future spectroscopic study of this state in :CHF and other halomethylenes.

3.2.2. *:CHCl/:CHBr/:CHI*

Spectroscopic study of :CHCl mirrors that of :CHF. However, the spectra of the heavier species are red-shifted from that of :CHF and, in their original report of the spectrum, Merer and Travis [25] were unable to follow the bending progression to the band origin because of poor Franck–Condon factors and a lack of sensitivity. The vibrational numbering was established by isotopic substitution of the hydrogen by deuterium. Analysis of the rotational structure also showed that the molecule is more nearly linear in the excited state compared to :CHF and an estimate of the energy of the barrier to linearity was made by application of Dixon's model [136]. The spectrum also displayed a classic example of axis-switching [137], resulting in the appearance of nominally forbidden rotational branches, due to the large geometry change between the two states involved in the transition. Again, matrix isolation infrared spectroscopy [138] established the ground state bending and C–Cl stretching vibrational frequencies, but relatively few further gas phase spectroscopic studies were reported [68,113] until the 1990s. Xu *et al.* [139] reported the observation of moderate resolution LIF spectra of several halocarbenes produced

in a hot nozzle source, but significant new spectroscopic information began to be obtained when Chang and Sears [73,74] applied newly developed, very sensitive, transient absorption techniques to the near-infrared region of the spectrum and obtained Doppler-limited spectra of the band origin and the first bending and C–Cl stretching excited bands, while the C–Cl stretching vibrational fundamental in the ground state was detected by mid-IR laser absorption [76].

Trends described above in the electronic spectrum of :CHF also occur in :CHCl. However, with the lower barrier to linearity in the latter, the onset of RT-induced reduction in intensity of vibronic transitions terminating in $\tilde{A}$-state levels with $K>0$ and perturbations in these same levels caused by the RT mixing of background $\tilde{X}$-state levels occurs at a lower excited state energy than in :CHF. The $\tilde{A}$-state vibronic level structure has been measured by a combination of absorption [70,71] and LIF excitation [87,97], but much work has focused on the ground state vibronic levels [97,140–142] with the aim of identifying the position of the triplet state via spin–orbit perturbations of singlet state levels and by direct detection of the perturbing triplet state vibronic structure. Most recently, stimulated emission pumping (SEP) [105] was used to measure the first rotationally resolved spectra of the triplet state levels. Table 1 summarises the current best experimental measurements for the vibrational fundamentals of :CHCl in both singlet states.

Potential surfaces for the three low-lying electronic states of :CHCl have been obtained both from a combination of purely *ab initio* theory [143] and a combination of *ab initio* calculations adjusted to precisely match experimentally measured vibronic intervals [144]. Estimated transition energies and intensities obtained from such surfaces have proved to be invaluable in assigning weak or hot bands in experimental spectra [70,105].

The spectroscopy of :CHBr has a shorter history as the first report of its electronic spectrum dates from the work of the Xu *et al.* [139] in 1994. Although a photoelectron spectrum of the negative ion [145] had been recorded previously, the experimental resolution was only adequate to barely separate vibrational intervals and the spectrum was complicated by the presence of multiple hot bands. The LIF spectrum obtained in 1994 was from a thermal decomposition of haloacetyl halides in a heated nozzle. Vibronic bands were resolved with partial resolution of the rotational structure, but a higher temperature background compromised the quality of the spectrum. Nonetheless, the data were sufficient to guide high-resolution studies at Brookhaven where Doppler-limited spectra at ambient temperature for several near-IR bands were detected soon after [75,77].

In the excited state the barrier to linearity [78,129] is lower than in either :CHF or :CHCl, and the onset of RT-like behaviour is evident even in the zero-point level of :CHBr, where the intensity of bands terminating in levels with $K>0$ is reduced and the upper state shows considerable rotational irregularity. Interestingly, :CDBr [72] shows more rotational sub-bands because the zero-point level is further below the barrier and the A rotational constant is smaller. The Brookhaven group continued work on the spectrum of :CHBr and :CDBr and measured the positions of many vibronic levels in both the $\tilde{A}$ and $\tilde{X}$ states by the analysis of Doppler-limited near-IR spectra close to the band origin [51,52]. Of particular interest was the first clear evidence for spin–orbit perturbation of the low-lying bending excited levels of the $\tilde{X}$ state [78], which was modelled using high-level

ab initio estimates of the coupling matrix elements to provide the first reliable experimental estimate of the triplet–singlet splitting in the halocarbenes. Building on this result, Tsai *et al*. [146] detected vibronic levels of the $\tilde{a}^3A''$ state in LIF DF of $\tilde{A}$ state levels. The normally forbidden singlet–triplet transitions gain intensity from the mixing of small amounts of singlet character into the triplet state levels. This aspect of the spectroscopy is discussed in more detail further.

Other hot band spectra led to the measurement of the C–Br stretching fundamental in the ground state [79] and the analysis of more recent DF spectra by the Chen *et al*. [147], Lee *et al*. [148] and Reid group [95,96] have established the vibronic levels up to several thousand wavenumbers of excitation in both singlet states as well as several spin–orbit mixed $\tilde{a}^3A''$ state levels so that a complete picture of the RT and spin–orbit perturbed pattern of vibronic levels in the multiple isotopic variants of this species is now available. Table 1 summarises the experimentally determined vibrational fundamentals. Franck–Condon factors for transitions involving changes in v_1 are rather small, although progressions involving the C–H stretch have been observed in the spectra of :CHF, :CHCl, and :CHBr.

Finally, we note that the last monohalocarbene, :CHI, has recently been spectroscopically detected [108] for the first time. The spectrum consists of a progression of bending and C–I stretching vibrations and the absolute vibrational numbering is not yet certain. Current work focuses on the determination of the band origin, and on the exact size of the triplet–singlet splitting. DF spectra indicate that the triplet origin lies approximately 1315 cm^{-1} above the zero-point level of the singlet ground state. All $\tilde{X}$ state bending vibrational levels above this energy are perturbed by spin–orbit coupling with the triplet manifold.

3.2.3. *:CCl_2 and other dihalocarbenes*

We restrict the scope of this article to include only selected species here. While the difluorocarbene radical, for example, is particularly stable and an electronic spectrum of it was reported in 1950 [20], both singlet states in :CF_2 are bent and the absorption or excitation spectra exhibit regular asymmetric top-like rotational structure at least up to moderate ($v_2 = 5$) [59] bending excitation. As in other halocarbenes, the spectrum is dominated by a long bending progression, but the RT effect is much less important in the accessible singlet absorption spectrum. At shorter wavelengths, the molecule dissociates. The trend in RT mixing of the singlet states in dihalocarbenes is neatly summarised in the measured fluorescence lifetimes of the excited state as reported by Huie *et al*. [149]. :CF_2 has a fluorescence lifetime of just 61 ns, :CFCl 644 ns and :CCl_2 3.81 ms. Correcting for the ν^3 frequency factor still results in a six-fold increase in lifetime for the dichloro species compared to the difluorocarbene – an observation at least partly explained by the increased RT mixing along the series. More recent measurements of the lifetimes [104] of different vibronic levels of CCl_2 have refined the numbers somewhat, but the essential picture remains.

By contrast to difluorocarbene, dichlorocarbene exhibits behaviour more closely related to the monohalocarbenes. The excited state barrier to linearity is some 6500 cm^{-1} above [104] the zero-point level of the $\tilde{A}$ state, similar to that of :CHF but considerably above that found in the :CHCl and :CHBr, and the lower energy section of the absorption/LIF excitation spectrum exhibits regular vibrational structure, albeit complicated by

considerable anharmonic coupling between vibrational levels. However, the onset of RT coupling clearly shows as sub-bands terminating in levels with $K>0$ lose intensity to shorter wavelengths, the A rotational constant increases, and the fluorescence lifetime for levels with higher K increases markedly. All of these observations mirror those seen in the mono-halocarbenes discussed above and we can be sure that, in $:CCl_2$, we are seeing the onset of strong RT coupling, just as expected. The location of the triplet $\tilde{a}\,^3A''$ state in $:CCl_2$ has not been identified, but it is certainly above that in :CHCl, since no evidence for it has been found in DF spectra up to 10,000 cm^{-1} above the zero-point level of the ground state [94]. More details are given in the next section.

Continuing the trend, the spectroscopy of $:CBr_2$ has recently received more attention, beginning with LIF excitation spectroscopy in a heated nozzle source [150], and more recently DF studies [99,100,151] aimed at locating the triplet state. The excitation spectrum shows the familiar extended bending progression complicated by anharmonic resonances with combinations of stretching vibrations. An improved production method and the diagnostic ^{79}Br and ^{81}Br isotope structure in the bending and bend-stretch progressions bands also recently permitted [152] a reassignment of the vibrational numbering in the excited state. The appearance of the excitation spectrum is very similar to the lower energy region of the dichloro species; combinations of the bending and symmetric stretching vibrations dominate and the progressions can be mostly fit using a standard Dunham expansion. As the spectrum is followed to higher energy, irregularities in the bending spacings and an increase in the A rotational constant indicate the approach to the barrier to linearity [100] around 3400 cm^{-1} above the zero-point level of the $\tilde{A}$ state. Predictions of the appearance of the spectrum based on *ab initio* calculations [153] of the potential surfaces were in good accord with the newest spectroscopic results.

DF studies [99,151] of CBr_2 have resulted in a map of ground state levels out to more than 6000 cm^{-1}. The most recent work [99] found that approximately 90% of the levels observed could be assigned to singlet state vibrational levels based on a simple Dunham expansion fit. No triplet state levels could be identified; however the DF spectra are congested and future higher resolution laser OODR work will be required to completely resolve the large level density seen at the energies of interest in this species.

The spectroscopy of the mixed fluorochloro- and fluorobromo-carbenes has also received considerable attention because of their relevance to stratospheric ozone depletion chemistry. In general, their spectra follow the trends exhibited by the monohalocarbenes and the dihalocarbenes discussed above. More electronegative atoms result in a shift of the singlet absorption spectrum to the blue, but the extended bending progressions remain, often with greater degrees of anharmonic resonance leading to more involvement of stretching activity in the observed spectra. As noted above, the general trend for longer fluorescence lifetimes of the origin band in heavier halocarbenes argues for some $\tilde{A}-\tilde{X}$ mixing, either by RT or spin–orbit mechanisms. However, in absorption/LIF excitation spectra, little evidence for the onset of strong RT coupling due to the approach to energy of the linear configuration is seen. Instead, the fluorescence lifetimes and spectral intensity begin to reduce at shorter wavelengths in both CFCl [57] and CFBr [43] and vibronic bands noticeably broaden, i.e. the molecule is predissociating before the energy of the linear configuration is reached. Vibrational assignments in the CFBr spectrum were very recently reassessed [154], and photodissociation dynamics remain of interest [44] and are described in more detail further.

3.3. *Spin–orbit coupling*

3.3.1. *:CHF (A state)*

Spin–orbit coupling in triatomic carbenes ranges from the situation in methylene, where the spin–orbit coupling is very weak and only isolated rotational levels are perturbed due to accidental near-degeneracies of singlet and triplet levels of the same symmetry [155] to that in molecules containing the heavier halogens where all the rotational levels in a given vibronic level are shifted [78]. The experimental evidence suggests that :CHF lies closer to the methylene limit. Polarisation quantum beat spectroscopy [90] of fully rotationally resolved levels in one component of the split $\tilde{A}\ ^1A''(040)$ level show extensive rotational perturbations. Measurements of effective hyperfine constants and *g*-factors by (Zeeman) quantum beat spectroscopy on a line-by-line basis provided a coherent picture of levels perturbed by a nearly degenerate set of triplet state levels probably following the model originally proposed by Stevens and Brand [156] for cases where the spin–orbit coupling matrix elements are small compared to typical vibronic level spacings, just as in the case of CH_2. Direct spin–orbit interaction between the $\tilde{a}$ and $\tilde{A}$ states is not possible because they possess, at least to a first approximation, the same electronic configuration, so the effect must be mediated by the RT interaction that causes the observed gross splitting in the level. Experimental estimates of the size of the coupling matrix elements were of the order of tenths of wavenumbers [90].

Lower in the vibrational manifold of $\tilde{A}$ state :CHF, Butcher *et al*. [81] identified small local perturbations in $\tilde{A}\ ^1A''(000)$ levels that were also attributed to spin–orbit mixing, but again no specific triplet background state could be identified as the one responsible. Despite a comprehensive search in a recent DF experiment [92], no evidence for triplet state level perturbations in the $\tilde{X}$ state was found. This is likely due to the small ^{19}F spin–orbit coupling compared to the heavier species where such effects have been noted. Detection of triplet–singlet perturbations and an exact measurement of the triplet–singlet splitting in :CHF awaits rotationally resolved, probably laser OODR, measurements of highly vibrationally excited $\tilde{X}$ state levels above the triplet zero-point level. Due to the sparsity of rovibronal levels low in the triplet manifold and the small spin–orbit coupling, we would expect to see few such perturbations at energies close to the triplet origin.

3.3.2. *:CHCl/CHBr*

Observation of spin–orbit perturbations in chloro- and bromo-methylene are intimately related to the determination of the triplet–singlet splitting in the molecules, which is discussed in detail futher. For both these species, the spin–orbit coupling is, unsurprisingly, significantly stronger than in :CHF or $:CH_2$ itself. Instead of locating individual perturbed rotational levels, one now finds gross shifts in vibrational level energies, and with sensitive spectroscopic techniques one can identify the triplet levels responsible for the perturbation and then determine the relative positions of the two states.

The effects were first noted in spectra of :CHBr and :CDBr [72,78] when the energies of the first few bending vibrational levels in the ground state of the isotopologues were found to be incommensurate. The observed pattern could only be explained by perturbation from another state which, at the energies involved, had to be the lowest triplet. By modelling the observed pattern of vibrational levels and *ab initio* calculation of the triplet surface and spin–orbit matrix elements [78] a prediction of the exact position

of the triplet state was made. Subsequent DF measurements by the Chang group [146,148] and one of us [95,96] confirmed the predictions, detected the triplet origin and estimated a spin–orbit matrix element of 330 cm^{-1} from a deperturbation analysis of the observed triplet zero-point energy. This is of the order of a hundred times larger than the typical spin–orbit matrix elements determined in the analysis of perturbations in the spectra of :CH_2, and :CHF.

The case of :CHCl is similar to that of :CHBr. Here, computational work by Tarczay *et al*. [143] and Yu *et al*. [144] made detailed predictions of the positions of the triplet state levels, and experimentalists, guided by these predictions and encouraged by success in :CHBr, detected both shifts in singlet levels and the triplet levels responsible for them by DF spectroscopy [97]. Spin–orbit coupling matrix elements were calculated [144] to be in the 80–120 cm^{-1} range, smaller than in :CHBr. This, together with the fact that the mutually perturbing levels turn out to be further apart in :CHCl than in :CHBr, results in smaller observed singlet vibrational level shifts and weaker spectral features associated with the triplet perturbing levels.

3.3.3. *:CHI*

LIF spectra of :CHI were reported only very recently [108] and represent the first observation of the electronic spectrum of iodocarbene. Although the analysis of the spectra is continuing, the DF spectrum shows a regular progression of bending and C–I stretching levels up to about 1500 cm^{-1} when extra peaks appear and the regularity is lost. These observations are explained by the appearance of the triplet origin and extensive spin–orbit mixing of triplet and bending singlet vibronic levels. Clearly, the spin–orbit coupling elements are larger here than in :CHBr and there are extensive mutual perturbations. Future work will focus on a quantitative deperturbation analysis of the levels and estimation of the spin–orbit matrix elements.

3.4. *Axis-tilting*

The earliest observations of high-resolution spectra of the halocarbenes by Merer and Travis [25,26] noted the appearance of parallel rotational sub-branches in a perpendicular electronic transition expected to include just perpendicular, *c*-type [128] rotational sub-branches. The explanation lies in the fact that in the singlet band system of the halocarbenes, the molecule undergoes a large change in geometry on excitation. The molecule fixed axis system, fixed by the Eckart conditions [128] by the geometry of each state, therefore changes on excitation. The effects of this 'axis-switch' were first investigated by Hougen and Watson [137] in the context of spectra of a number of small species including HSiCl and HSiBr 2 years before Merer and Travis's reports. The axis rotation linking the Eckart frames in the two states means that the definition of the symmetric top projection quantum number, K, in the two states is different, leading to the observation of unexpected rotational sub-bands in the spectrum. As Hougen and Watson noted, these 'effects are most noticeable in [the spectra of] near symmetric tops'. For triatomic species such as those we are concerned with, the rotation matrix linking the upper and lower state molecule-fixed frames is simply a rotation (or tilt) about the out-of-plane axis and it has the effect of scrambling the definition of K, mixing odd and

even K levels. This leads to the appearance of a prominent ${}^{Q}Q_0$ branch in many halocarbene spectra, which gains its intensity from mixing of $K=1$ character into $K=0$ rotational functions when the orientation of one state's axis system is rotated into the other.

Lin *et al*. [71] made careful measurements of rotational branch intensities in the origin bands of :CHCl and :CDCl in order to assess the accuracy of the Hougen and Watson model describing axis-switching, because there were indications that the floppy nature of the bending vibration in the excited state could cause it to break down. The model implicitly assumes small amplitude harmonic displacements in a rigid rotor framework. In addition, *c*-type Coriolis coupling offers a second mechanism to explain the observation of the parallel sub-bands and experimental measurements can assess the magnitude of the two possible contributions.

In the end, Lin *et al*. showed that a combination of axis-switching modelled according to the Hougen and Watson model, plus exact *ab initio* calculation of the Coriolis coupling coefficients resulted in calculated relative intensities of the parallel and perpendicular bands that agreed very well with the measurements. Additionally, it was found that the *c*-type Coriolis' contribution to the observed intensities was less than 1% of the axis-switching one in this case, although the former would be expected to increase with additional bending excitation in the excited state.

To investigate this point, Hall *et al*. [118] repeated the experiment for the (060)–(000) band of :CHBr in the visible region. Here, the relative intensity of the parallel sub-bands was found to be much larger than can be accounted for by axis-switching alone, or by axis-switching combined with *c*-type Coriolis coupling of any reasonable size. It was also not possible to accommodate the strength of the observed transitions assuming a large amplitude bending model. It was postulated that intensity borrowing from the next higher $\tilde{B}^1A'$state was contributing to the observed parallel intensities. This state has not been detected in :CHBr, but is known for CH_2 [157,158] and very recently detected in :CHF and :CHCl (below). For :CHBr the $\tilde{B}-\tilde{X}$ origin is predicted [118] to lie near 21,000 cm^{-1}, some 4000 cm^{-1} above the energy of the $\tilde{A}(060)$ level.

3.5. *Other perturbations/higher excited states*

In the previous section, we noted that observed spectral intensities in higher vibrational bands of the spectrum of :CHBr might be explained by intensity borrowing from the $\tilde{B}-\tilde{X}$ transition. The same mechanism would be operative in the other halocarbenes, and some effort has been made in searching for the second excited singlet state. So far, only in :CHF and :CHCl has this been successful [103] and, in this case, all the observed $\tilde{B}$ state vibrational levels are found to be lifetime broadened, presumably due to predissociation. In the analogous state of CH_2, lower lying vibrational levels of the $\tilde{C}^1A'$ state which are below the molecule's singlet dissociation limit have been identified, but predissociation broadening is observed at the first bending vibrational level above the dissociation threshold [119]. Future investigations based on, for example, action spectra of the dissociation product, could make use of the known predissociating levels in :CHF and :CHCl and form the basis for a spectroscopic determination of the bond dissociation energy. More discussion of the photochemistry of these species is included in Section 5.

4. The singlet–triplet gap in halocarbenes

The singlet–triplet gap (ΔE_{ST}) and its dependence on steric and electronic effects represent the oldest and most intriguing issues regarding carbenes. As the smallest carbenes with singlet ground states, the halocarbenes are model systems for experimental studies of the singlet–triplet gap and afford ready comparison with predictions of high-level *ab initio* theory. Indeed, over the past several decades the halocarbenes have served as important theoretical benchmarks for carbene singlet–triplet gaps, with over 40 studies appearing on the topic, using a wide variety of theoretical methods [9,43,143,144,153,159–196]. Experimental studies have lagged behind; however, a number of studies of ΔE_{ST} for the halocarbenes have appeared in recent years, using a variety of experimental techniques, including: (a) negative ion PES, (b) hot-band absorption, (c) emission spectroscopy and (d) SEP spectroscopy. We will address each of these in turn.

4.1. *Negative ion PES*

An innovative method to determine the singlet–triplet gaps of halocarbenes based upon PES of the corresponding negative ion was implemented in the late 1980s by Lineberger and co-workers [145,197,198]. In this method a molecular beam containing the negative ion of the desired carbene is prepared in an electron impact source and mass-selected. The electron is photodetached by laser excitation, and the kinetic energy distribution of the resulting photoelectrons is measured. In principle, detachment into the singlet and triplet states of the neutral can be readily inferred from the photoelectron spectrum. In practice, the large geometry change between anion and neutral often leads to extensive vibrational progressions in the PE spectrum, which requires detailed Franck–Condon analysis and complicates the identification of the electronic origins. Thus, the negative ion photoelectron studies have yielded mixed results when compared with predictions of *ab initio* theory and other experimental techniques.

In 1988, Lineberger and co-workers reported their initial PES studies of the negative ions HCF^-, $HCCl^-$, $HCBr^-$, HCl^-, CF_2^- and CCl_2^- [197]. Upper bounds on ΔE_{ST} for the monohalocarbenes :CHF, :CHCl, :CHBr and :CHI were set, which were in good agreement with available *ab initio* studies at that time. Limited information was obtained regarding ΔE_{ST} of the dihalocarbenes; however, a lower bound on ΔE_{ST} for $:CF_2$ of $209(8)\,kJ\,mol^{-1}$ was determined, which is in good agreement with theory and a prior experimental result from emission spectroscopy (see below for details) [199–201]. Note that in the notation used here, a positive value of ΔE_{ST} implies a singlet ground state.

In 1992, the same group reported new negative ion PE spectra of the monohalocarbene anions. By taking spectra with parallel and perpendicular orientations of the laser polarisation vector and detection axis, they were better able to resolve the overlapping singlet and triplet transitions. For CHF, the determined ΔE_{ST} was $62.3(17)\,kJ\,mol^{-1}$, in excellent agreement with theory, and even today this stands as the best experimental value for the singlet–triplet gap of fluorocarbene. In contrast, estimates for the heavier halocarbenes had significantly larger error bars due to the greater overlap of the singlet and triplet spectra. Derived ΔE_{ST} values (in $kJ\,mol^{-1}$, with experimental uncertainty in parenthesis) were: 18(11) for :CHCl, 11(9) for :CHBr and −17 to −42 for :CHI. Considering the uncertainties, the values obtained for :CHCl and :CHBr were in agreement with available theoretical values [165–167]. At the time of the 1992 paper,

no theoretical studies had yet calculated ΔE_{ST} for :CHI; however, in the wake of this experimental several theoretical papers on the subject promptly appeared. Thus, in 1993 Russo *et al.* reported a ΔE_{ST} of 15.5 kJ mol^{-1} using the LCGTO-LSD method [174], and subsequent studies obtained similar results [173,177,179,181] revealing a significant discrepancy between experiment and theory.

This discrepancy expanded significantly in 1999, with a report from the Lineberger group regarding negative ion PE spectra of the symmetric dihalocarbene anions CF_2^-, CCl_2^-, CBr_2^- and CI_2^- [198]. This study provided an improved value for the ΔE_{ST} of :CF_2 of 226(13) kcal mol^{-1}, which is in good agreement with theory and prior experiments [199–201]. However, reported ΔE_{ST} values for the heavier halocarbenes were much smaller (in kJ mol^{-1}): 13(13) for :CCl_2, 4(13) for :CBr_2 and −4(13) for :CI_2. This implied that ΔE_{ST} for :CCl_2 was similar to or smaller than that of :CHCl, a quite striking result! Moreover, these values were in significant disagreement with the available (and by now expanded) set of theoretical values. For example, roughly 10 theoretical predictions of ΔE_{ST} for :CCl_2 were available at that time [162,166,168,169,171,172,176,194,195], all of which gave values between 56.5 and 108.4 kJ mol^{-1}. The average value of ~88 kJ mol^{-1} was seven times larger than experiment, and it was suggested that theory was overstabilising the singlet state [198]. More theoretical studies followed, all of which gave a similar value for ΔE_{ST}, and several even attempted to explain the discrepancy – the most popular explanation being that the experimental results were contaminated by a low-lying quartet state of the anion [193,196]. Very recently, the Lineberger group has re-examined the negative ion PES of CCl_2^- and discovered a significant contamination from $CHCl_2^-$ as a result of the limited resolution of their mass gate, which accounts for most of the signal assigned to triplet bands in the previous work. The revised experimental value for ΔE_{ST} of :CCl_2 is now in good accord with theory.

The remaining discrepancy between the negative ion PE results and theory concerns ΔE_{ST} of the iodocarbenes, particularly CHI. This discrepancy has finally been resolved via the use of emission spectroscopy, as we describe in detail further.

4.2. *Hot-band absorption spectroscopy*

For the heavier halocarbenes, the singlet–triplet gaps are small enough so that even low-lying vibrational levels of S_0 experience perturbations from spin–orbit interaction with nearby T_1 levels. Thus, measurement of perturbations in the singlet level positions is a sensitive probe of this coupling. In favourable cases, this can be achieved via emission spectroscopy, as detailed further. However, one of us (T.J. Sears) reported an innovative approach to examine singlet–triplet interactions and the singlet–triplet gap in halocarbenes by measuring hot-band spectra from vibrationally excited singlet levels that are perturbed by neighbouring levels of the triplet state [78].

This approach was first utilised to measure spectra from excited bending levels in :CHBr and :CDBr [78]. Transitions which originated in levels with up to two quanta of bend were measured. Due to the significant bond angle change between S_0 and T_1 (Figures 1 and 2), vibrational overlaps with T_1 are largest for the bending levels of S_0, and consequently these are the most perturbed. Their results showed that the first bending overtone, or (0, 2, 0), in :CHBr was significantly perturbed, with the only plausible perturber being the vibrationless level of the triplet. Comparisons with extensive *ab initio*

calculations that incorporated spin–orbit coupling between S_0 and T_1 reproduced the pattern of perturbations in the singlet level structure, and suggested a triplet excitation energy [$T_{00}(\tilde{a} - \tilde{X})$] of $\sim$2028 cm^{-1} ($\sim$24.3 kJ mol^{-1}). A similar approach applied to :CHCl met with less success [70], as in this case the triplet origin lay higher in energy.

4.3. *Emission spectroscopy*

The very first spectroscopic measurement of the singlet–triplet gap in a halocarbene was reported by Koda, who observed T_1–S_0 emission following chemical production of triplet :CF_2, and determined $\Delta E_{ST} = 236$ kJ mol^{-1}. As noted above, this value is in excellent agreement with the negative ion PES results [198], and with theory.

In 2001, Chang and co-workers applied SVL emission spectroscopy to probe the low-lying vibrational structure of :CHBr and :CHCl, generated using a pulsed discharge nozzle [140,146]. For :CHBr, they found a highly perturbed level structure in the singlet manifold, with a larger density of observed states which could arise solely from that manifold. The triplet origin was assigned to a band at 2006 cm^{-1}, which implied a ΔE_{ST} of 23.8(12) kJ mol^{-1}. This value was in good agreement with theory [162,164–169,171–173, 176,181–184,195], but in poor agreement with the negative ion PES measurement [145]. Later that same year, the authors extended these studies to :CDBr [147] and :CHCl [140]. For the latter, no perturbations in the singlet vibrational structure were observed up to an energy of roughly 33 kJ mol^{-1}, which was set as a lower limit on the singlet–triplet gap. Subsequent studies of :CHCl and :CDCl using a more sensitive CCD detector [142,202] revealed very weak transitions which were assigned to levels of the triplet state based upon theoretical predictions [142]. The singlet–triplet gap was determined to be 25.9(2) kJ mol^{-1} for :CHCl and 26.2(2) kcal mol^{-1} for :CDCl. These values were again in good agreement with theory [143,144,162,164–169,171–173,176,181–184,186,194–196] and within the uncertainty of the negative ion PES measurement [145].

Extension of the emission studies to examine the singlet–triplet gap of the dihalocarbenes was less successful. In 2005, Chang and co-workers reported studies of :CBr_2 [151], where transitions to the triplet state could not be clearly identified. However, an increased level density was noted beginning at around 3650 cm^{-1} (43.7 kJ mol^{-1}), and attributed to levels of the triplet state. A similar approach was applied to :CCl_2 [203], and unassigned lines observed at energies >5000 cm^{-1} above the singlet origin were tentatively assigned to levels of the triplet state. Later, tentative assignments of the triplet levels were given based upon high-level *ab initio* calculations which included the effects of anharmonicity [143].

In an effort to resolve some of the issues involved in the dihalocarbene singlet–triplet gaps, and as a prelude to double resonance experiments, one of us (S.A. Reid) in 2005 initiated extensive studies of the mono- and dihalocarbenes using SVL emission spectroscopy [92,94–97,99,101,102,108]. For the monohalocarbenes, following studies of the excitation spectra which identified progressions involving all three modes, we measured emission spectra that fully characterised the vibrational level structure of the singlet and (in the case of :CHCl, :CDCl, :CHBr, and :CDBr) triplet manifolds. Very recently, we successfully recorded fluorescence excitation and emission spectra of :CHI for the first time [108], and our results confirmed a singlet multiplicity for the ground state with

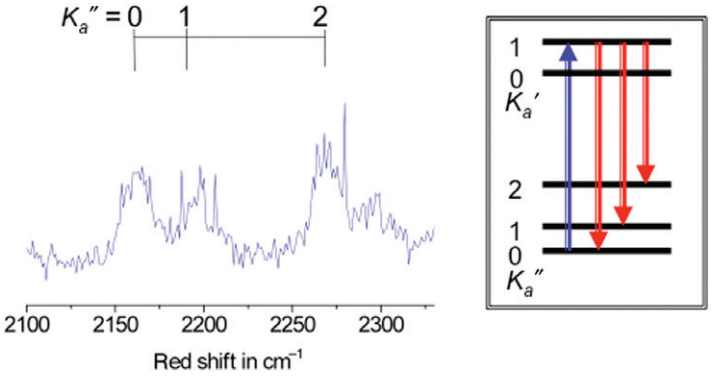

Figure 6. [Colour online] SVL emission spectrum of the triplet origin band of :CH^{35}Cl, obtained by pumping an upper state level with $K_a = 1$. The resulting spectrum contains both parallel ($\Delta K_a = 0$) and perpendicular ($\Delta K_a = \pm 1$) components, as expected for a singlet–triplet A''–A'' transition.

a lower bound set on ΔE_{ST} of 15.7 kJ mol^{-1}, in excellent agreement with theory [174,181,185], but markedly different than the negative ion PES result [145].

Extending our studies to the dihalocarbenes, in 2006 we utilised K_a-sorted emission spectra to probe for triplet levels in :CCl_2. This approach exploits the large change in bond angle between S_0 and T_1, which leads to a much larger A rotational constant for the latter. Taking :CHCl as an example, this constant is around 65% larger for T_1 than S_0. By pumping excited K_a levels in the excitation spectrum, and taking advantage of the $\Delta K_a = \pm 1$ selection rule in this perpendicular transition, the splitting of K_a levels in the emission spectrum affords a rough determination of the A constant (actually $\tilde{A} - \bar{B}$) for levels in this ground state. This approach had been used earlier to confirm the triplet origin assignment in :CHCl (Figure 6) [97]. At energies of 3500–9000 cm^{-1} above the vibrationless level of S_1, only a modest increase in $\tilde{A} - \bar{B}$ was found, and ~86% of the observed lines between 5000 and 9000 cm^{-1} could be assigned to levels of S_0. Subsequent studies of :CBr_2 and :CBrCl also failed to identify triplet levels or triplet-induced perturbations in the singlet manifold [99,101]. A possible explanation for this lack of success is the higher ΔE_{ST} for the dihalocarbenes, which means that the triplet origin is isoenergetic with highly excited vibrational levels of S_0, for which the vibrational overlaps are poor.

4.4. *SEP spectroscopy*

SEP spectroscopy, originally developed by Field and co-workers [204], is a versatile method that has been successfully applied to the spectroscopy of transient species [205]. In this method, illustrated in Figure 7, an intense (DUMP) laser pulse is used to stimulate emission from an electronically excited state prepared by laser excitation (PUMP). The advantages of this method over SVL emission spectroscopy are three-fold [205]: (1) the double resonance nature of the experiment results in a significant spectra simplification, due to the rotational selection rules active in each step, (2) the resolution is laser limited

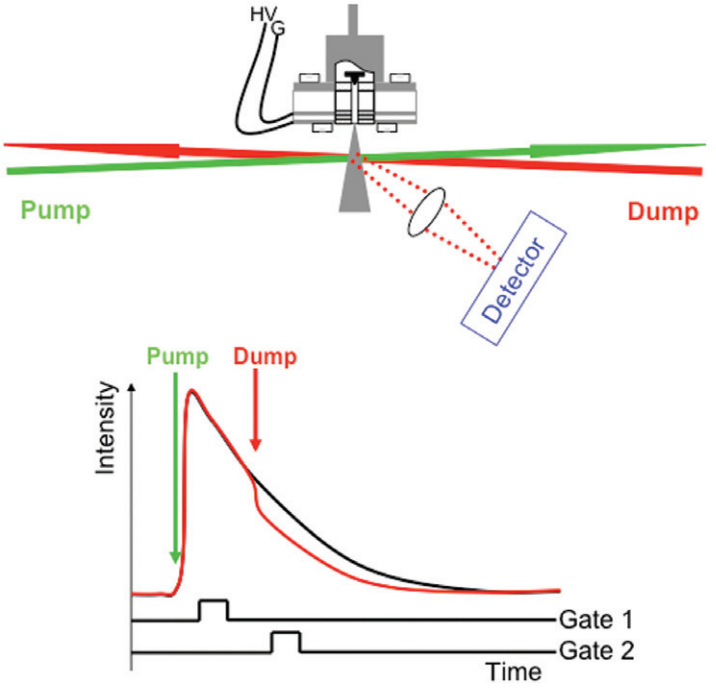

Figure 7. [Colour online] Illustration of the SEP technique applied to probe the singlet–triplet gap and spin–orbit perturbations between the lowest singlet and triplet states in halocarbenes with rotational state resolution. Our approach uses the common dual-gated scheme to measure the depletion in spontaneous emission induced by the DUMP laser.

and (3) the intense DUMP pulse can be used to enhance weak transitions (while, of course, saturating strong ones).

The first application of SEP to a halocarbene was the seminal experiment of Suzuki and Hirota [132], who obtained SEP spectra of low-lying vibrational levels of :CHF and examined anharmonic interactions among these levels. However, the energies accessed in their experiment did not encompass the region of the triplet state. One of us (S.A. Reid) has explored the higher energy region using both SVL emission [92] and SEP spectroscopy [107], and despite having a good prediction of the triplet position from the negative ion PES measurement [145] no transitions to triplet levels have been identified. We conclude that the spin–orbit coupling is too weak in this system for the triplet levels to gain sufficient oscillator strength, a suggestion supported by the very weak triplet transitions observed in SVL emission spectra of the heavier halocarbene, :CHCl [97,142].

Very recently, we applied the SEP method to :CHCl and :CDCl for the first time [105,106]. The SVL emission experiments had identified the position of the triplet origin (and several vibrationally excited triplet levels) to within several cm^{-1}; however, these assignments were based only on the excellent match with theoretical predictions, and we desired to obtain further information on the structure of the triplet state and the singlet–triplet gap from rotationally resolved studies. Our SEP studies (Figure 8) gave the first rotationally resolved spectrum of singlet–triplet transitions in a halocarbene. The spectra

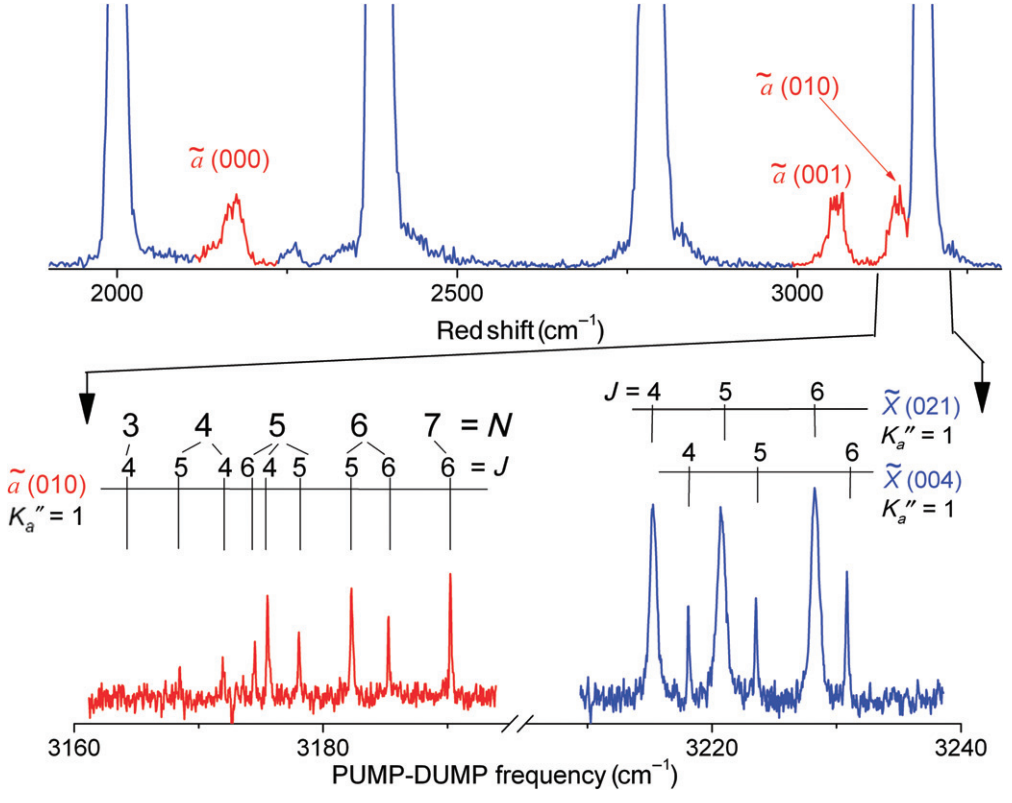

Figure 8. [Colour online] Rotationally resolved spectra of singlet and triplet levels in :CH^{35}Cl measured using SVL emission (upper panel) and SEP spectroscopy (lower panel). The rotationally resolved SEP spectra of singlet levels displays a simple three line pattern reflecting the ($\Delta J = 0, \pm 1$) selection rules. In contrast, the triplet spectrum displays a nine line pattern which reflects the coupling of spin and rotational angular momenta. This reflects the first rotationally resolved spectra of singlet–triplet transitions in a carbene.

were analysed using a modified version of the STROTA program of Judge [105,106], and the rotational constants derived from this analysis were in excellent agreement with theory. It is astonishing that the precise ΔE_{ST} determined from this work for CH^{35}Cl, 2163.28(5) cm^{-1} or 25.8789(8) kJ mol^{-1}, is within several cm^{-1} of recent high-level *ab initio* predictions [143,144]! Analysis showed that among the spin interactions the spin–spin interaction was dominant, with a primary contribution (to second order) from mixing with nearby singlet levels. This was further evidenced in the pronounced vibrational state dependence of the spin–spin coupling constant, from which first the vibronic and, finally, purely electronic spin–orbit coupling matrix elements were obtained, which is in excellent agreement with theoretical predictions [106].

In concluding this section on halocarbene singlet–triplet gaps, we summarise in Table 2 information regarding the singlet–triplet gaps of the halocarbenes. At the outset of this review, we noted that theory had often led experiment regarding the singlet–triplet gap of the halocarbenes. This is shown in Figure 9, which displays a comparison of experimental

Table 2. Summary of experimental and selected theoretical values for the singlet–triplet gap of the mono- and symmetric di-halocarbenes.

Carbene	ΔE_{ST} (experiment)[a]	Ref.	ΔE_{ST} (theory)	Ref.
:CHF	62.3(17)	[145]	55.2	[165]
			66.1	[169]
			56.1, 59.0	[177]
			59.8	[181]
:CHCl	25.9789(8)	[106]	25.9, 28.0	[177]
	25.9(2)	[142]	23.7	[181]
	18(11)	[145]	25.9	[143]
			25.86	[144]
:CHBr	23.8(12)	[146]	17.2	[165]
	24.3	[202]	20.0	[181]
	11(9)	[145]	21.9	[78]
			27.2, 29.7	[177]
:CHI	>15.7	[108]	15.5	[174]
	−17 to −42	[145]	20.1, 22.2	[177]
			12.6	[181]
			13.4, 18.8	[185]
$:CF_2$	236	[199]	226, 227	[177]
	226(13)	[198]	234	[181]
			227, 235	[185]
$:CCl_2$	13(13)[b]	[198]	82.0	[181]
			79.5, 82.8	[185]
			84.1	[143]
$:CBr_2$	4(13)[b]	[198]	63.2	[181]
			63.6, 67.4	[185]
$:CI_2$	−4(13)[b]	[198]	36.8	[181]
			48.1, 49.4	[185]

Notes: [a]Positive value implies singlet ground state. All values are in kJ mol^{-1}. Numbers in parenthesis are the estimated measurement errors in units of the least significant figure.
[b]These experimental values have been called into question, and we consider the theoretical values to be more reliable.

and theoretical values for the singlet–triplet gap of CHCl over the past 25 years. Although there is some spread in the theoretical results, clearly theory has had this correct all along! We should also note that, while the negative ion PES results have provided valuable information and are in a sense complementary to the other methods described here, there remains a significant discrepancy between those results and the ones from emission/SEP spectroscopy for :CHCl, :CHBr, and :CHI. The latter are in uniformly good agreement with theoretical predictions.

5. Halocarbene photochemistry

The preceding sections have concentrated on the complex spectroscopy of halocarbenes, which is brought about by the RT and spin–orbit interactions that mix the $\tilde{X}$, $\tilde{a}$

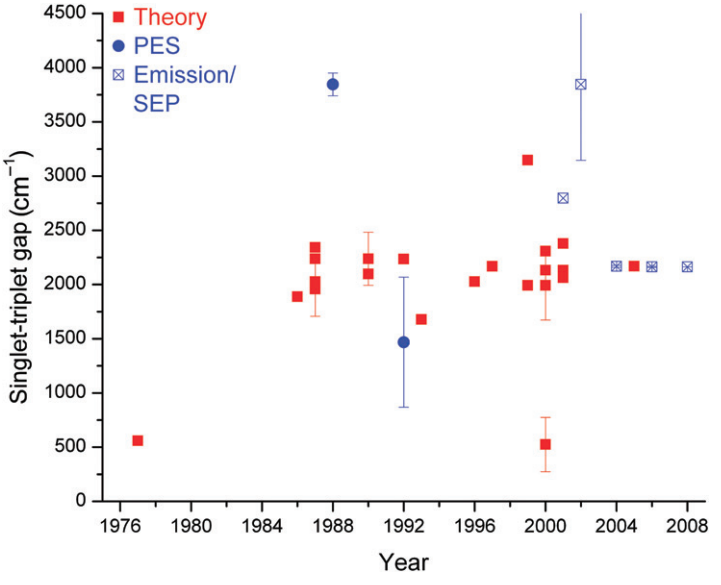

Figure 9. [Colour online] Evolution of experimental and theoretical values for the singlet–triplet gap of chlorocarbene (:CHCl) over the past several decades.

and $\tilde{A}$ states. This mixing is a strong function of bond angle and therefore the equilibrium bond angle and bending frequencies in the electronic states provide insight into the strength of these interactions. The focus of this section is on excitation of the bond stretching coordinates, leading, ultimately, to dissociation of the triatomic carbene into a halogen or hydrogen atom and a (halo)methylidyne radical. Unlike the rich spectroscopic history of carbenes, which stretches back more than half a century, studies of the photochemistry of carbenes – both theoretical and experimental – is little more than a decade old, with the first report of photodissociation of :CH_2 appearing in 1995 [206] and a halocarbene, :CFBr, in 1999 [44].

Figure 10 shows the four valence states of a general halocarbene, :CXY, as in Figure 2, but plotting the energy with respect to the C–X stretching coordinate. The upper panel shows the energies of the states at linearity, where the $\tilde{X}$ and $\tilde{A}$ states of the bent molecule are degenerate, correlating with the components of a $^1\Delta$ state. This state correlates with the halomethylidyne, CY, in its $^2\Delta$ excited state, along with a ground state hydrogen or halogen atom, X. The $\tilde{B}$ $^1\Sigma$ state correlates with CY($^2\Sigma^+$) while the $\tilde{a}$ $^3\Sigma$ state, which is the lowest energy at linearity, correlates with an excited quartet state, $^4\Sigma^-$product. The ground, $^2\Pi$, state of CY does not correlate with a bound carbene state. The order of the states of CY depends on which (halogen/hydrogen) atom Y represents; that shown in Figure 10 is appropriate (although not to scale) for CH and CCl. In CF, the $^2\Sigma^+$ state lies above the $^2\Delta$ state [207].

As the molecule bends, the orbitally degenerate states resolve into A' and A'' components (A_1 and B_1 for symmetric carbenes), as shown in the lower panel of Figure 10. The A' and A'' components of the $^2\Delta$ state interact with the A' and A'' components of the repulsive $^2\Pi$ state causing the $\tilde{X}$ and $\tilde{A}$ states to correlate, adiabatically, with ground state products. Generally, a small barrier remains on the $\tilde{A}$ $^1A''$ state potential, while the

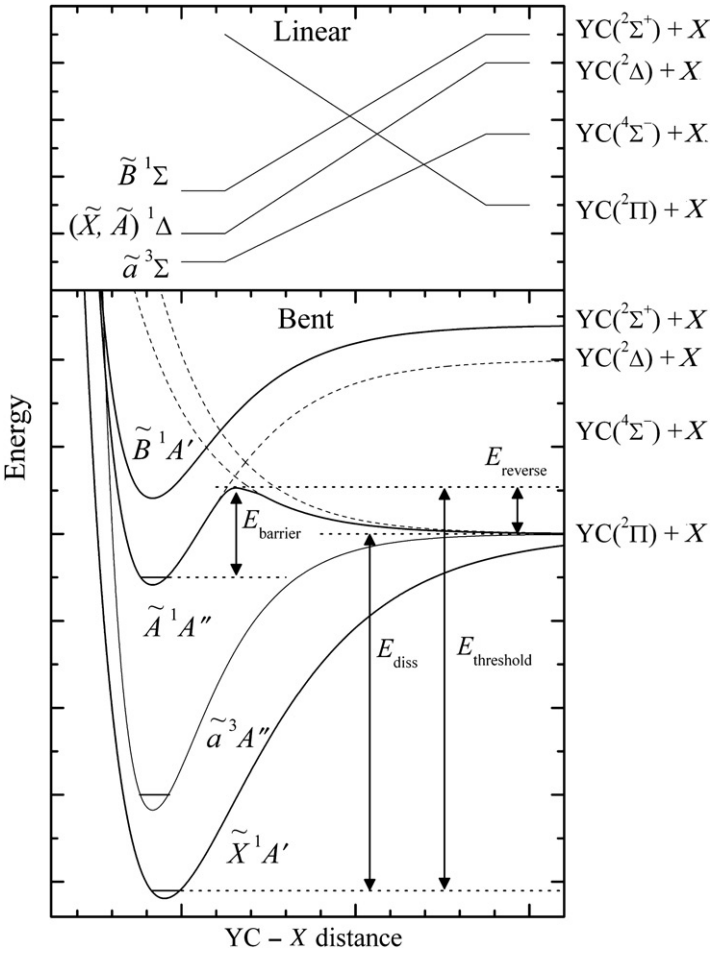

Figure 10. Illustrative examples of the lowest four valence states of a general halocarbene, :CXY at linear and bent geometries. Correlations with different states of the dissociation products, CY + X, are indicated. The definition of various energies used throughout the text is included.

$\tilde{X}^1A'$ state is barrierless. This barrier on the $\tilde{A}$ state has been calculated for all halocarbenes [42,43,80,109,153,186,191,208] and experimentally measured in a couple of instances (see below). The $B\,^1\Sigma$ state correlates with excited state products ($^2\Sigma^+$). Nothing is known, experimentally or theoretically, about the non-adiabatic interactions of this state. Experimentally, the $\tilde{B}$ state of :CHF, :CDF and :CHCl is predissociative, however, the mechanism of this predissociation is unknown (see further). In Figure 10 a couple of dissociative states are shown crossing the $\tilde{B}$ state, but no barrier is drawn, reflecting the unknown nature of this interaction. The $\tilde{a}\,^3A''$ state likewise interacts with the A'' and A' components of the $^2\Pi$ state allowing the triplet to correlate, adiabatically, with ground state products. It is not known whether this avoided crossing produces a barrier or not.

Despite the considerable spectroscopic exploration of halocarbenes, there has been comparatively little systematic study of the photochemistry induced by breaking this

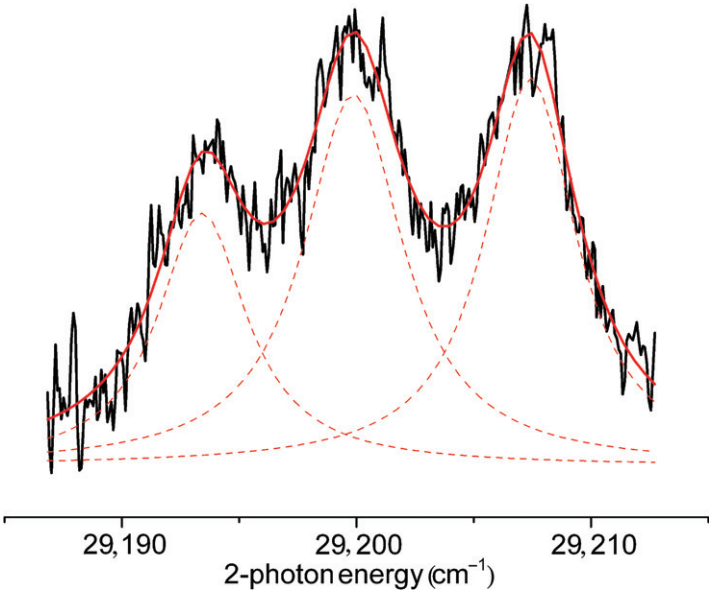

Figure 11. [Colour online] Rotationally resolved OODR spectra of a level in the $\tilde{B}$ state of :CD^{35}Cl. The rotationally resolved OODR spectra displays a simple three line pattern reflecting the ($\Delta J = 0, \pm 1$) selection rule. The upper state levels are significantly broadened by dissocation; the Lorentzian fits shown in the figure return linewidths of $\sim$5 cm^{-1}, corresponding to an upper state lifetime of $\sim$1 ps.

carbon–halogen (or hydrogen) bond. Via $\tilde{A}$ state excitation, only the photodissociation of :CFBr and :CFCl has been reported; CF fragments were explicitly probed for :CFBr [44], but only inferred in :CFCl. [57] $\tilde{B}$ state predissociation has been explored in :CHF, :CDF and :CHCl (Figure 11) [103,209] showing rotational and vibrational state-dependent linewidths, but the states involved and even the identity of the reaction products formed as a result of this predissociation are unknown. :CCl_2, :CHCl, :CFCl and :CFBr have been photodissociated at 193 and/or 248 nm [45–48,210,211]. This time the chemical products are clear, but the states involved are not (the initial state is presumably a Rydberg state). The most systematic study of the critical energies for photodissociation of carbenes, especially from the $\tilde{A}$ state, instead comes from theory [42,43,80,109,153,186,191,208]. Below, we examine first these theoretical energies, in comparison with other critical energies. We then examine the available experimental data, separated by initial state.

5.1. *Theoretical studies*

Table 3 lists, for all non-iodine containing halocarbenes, *ab initio* calculations of the energy of the RT intersection (E_{RT}), the thermochemical dissociation energy of the weakest C–X bond (E_{diss}), the height of the reverse barrier on the $\tilde{A}$ state (E_{rev}) and the barrier height on the $\tilde{A}$ state relative to the zero-point level of the $\tilde{X}$ state ($E_{threshold}$) and $\tilde{A}$ state ($E_{barrier}$). The definition of these energies is included in Figures 2 and 10. The values in the table are exclusively the work of Bacskay and co-workers [42,43,80,109,153,186,191,208].

Table 3. Calculated barriers to linearity (RT intersection) and dissociation on the $\tilde{A}$ states of all non-iodine-containing halocarbenes (energies in kJ mol^{-1}).

Halocarbene	E_{RT}	Channel	$E_{threshold}$	E_{diss}	$E_{barrier}$	$E_{reverse}$	Ref.
:CHF	285	CF + H	329	310	132	19	[109]
:CHCl	164	CCl + H	334	326	177	8	[186]
		CH + Cl	386	386	230	0	[186]
:CHBr	175	CH + Br	329	329	186	0	[212]
		CBr + H	342	335	199	8	[212]
:CF_2	Not found[a]	CF + F	550	511	95	39	[153,212]
:CFCl	386	CF + Cl	346	328	33	17	[186]
:CFBr	357	CF + Br	259	247	41	12	[44]
:CCl_2	279	CCl + Cl	324	319	108	5	[153]
:CClBr	261	CCl + Br	262	258	73	4	[191]
:CBr_2	228	CBr + Br	270	270	88	0	[153]

Note: [a]The RT intersection was found not to be a first-order saddle point.

While there are several later and more accurate calculations of electronic energies, equilibrium geometries and vibrational frequencies, there are no, more recent, calculations of the RT energy or the barrier to dissociation on the $\tilde{A}$ state. In addition, the values in the table have the advantage of using a consistent theoretical approach and so provide an excellent relative picture across the set of halocarbenes.

In brief, the calculations were carried out at several levels of theory, including Complete Active Space Self-Consistent Field (CASSCF), CAS-Second order Perturbation Theory (CASPT2) and Coupled Cluster with Singles, Doubles and perturbative Triples (CCSD(T)). The basis set for the calculations was Dunning's correlation consistent polarised valence triple zeta basis: cc-pVTZ, with the larger quadruple zeta basis used for dissociation energies with the coupled cluster methods. The thermochemical dissociation energies in the table, E_{diss}, are the best CCSD(T) calculations. CASPT2 was used to calculate the reverse barrier, E_{rev}, and the sum of these values then constitutes the best estimate of the photochemical threshold for dissociation on the $\tilde{A}$ state, $E_{threshold}$. The barrier height on the $\tilde{A}$ state, $E_{barrier}$, was calculated as the difference between $E_{threshold}$ and the $\tilde{A}$ state zero-point level, which was calculated using MRCI with Davidson correction. The reader is referred to the original papers for a full description of the theoretical methodology. Whilst putting this review together it became apparent that some values in the table were missing, in particular photodissociation barrier energies for the symmetric halocarbenes, the RT energy for :CFBr, and all values for :CHBr. Prof. Bacskay calculated these missing values for this review; the methods and discussion of these new values will be published separately [212].

The energies in the table vary widely: E_{RT} varies from 164 kJ mol^{-1} in :CHCl to 386 kJ mol^{-1} in :CFCl; E_{diss} varies from 247 kJ mol^{-1} for :CFBr to 511 kJ mol^{-1} for CF_2. $E_{threshold}$ is often slightly in excess of E_{diss} because of the small barrier in the exit channel formed from the avoided crossing as discussed earlier. The most important energies for photodissociation dynamics are $E_{barrier}$ and E_{rev}. Most of the halocarbenes have relatively deep potential energy wells in the $\tilde{A}$ state. Carbenes with $E_{barrier} > 100$ kJ mol^{-1} have vibrational states in the region of the barrier that are inaccessible from the ground

state (zero-point level) due to weak Franck–Condon factors. Even in :CBrCl, with a lower $E_{barrier} = 73\,kJ\,mol^{-1}$, the fluorescence excitation spectrum becomes too weak to observe just before the critical energy of the barrier is reached [213]. The fluorocarbenes, :CFCl and :CFBr, have the two lowest dissociation barriers in the table. There is a small reverse barrier for most carbenes, which implies that several bound $\tilde{A}$ state levels lie above the thermodynamic dissociation energy and hence are technically pre-dissociative. This is a very important distinction. When RT or spin–orbit coupling mixes the $\tilde{A}$ state with either the $\tilde{X}$ or $\tilde{a}$ state, the fluorescence lifetime of many vibrational states is significantly *lengthened* (see above). However, coupling of the predissociative $\tilde{A}$ state levels to the $\tilde{X}$ or $\tilde{a}$ state would lead to dissociation and hence significant lifetime *shortening*. As shown below, this is exactly what is observed.

5.2. *Photochemistry of the $\tilde{A}$ state*

5.2.1. *:CFBr*

The first halocarbene to be explored photochemically was :CFBr [44], which according to Table 3 has the lowest barrier to dissociation on the $\tilde{A}$ state that lies within the Franck–Condon region. The fluorescence excitation spectrum of jet-cooled :CFBr is shown in the upper panel of Figure 12 [43]. In comparison with the very long and symmetric progression in the bending mode exhibited by :CHF in Figure 5, the progressions in :CFBr are truncated suddenly near $3000\,cm^{-1}$ ($36\,kJ\,mol^{-1}$) of vibrational energy. Fluorescence lifetimes have also been measured for several of the states, some of which are indicated in the figure. Most of the strong peaks have lifetimes, $\tau \approx 1\,\mu s$. The lifetime shortens considerably at the end of the spectrum with the last peak exhibiting τ 100 ns. Some of the smaller peaks in the spectrum also appear to have shortened lifetimes, an observation to which we shall return later. The shortening of fluorescence lifetime indicates coupling to a dissociative state, and the close agreement between the energy of the last vibrational state and the value for $E_{barrier} = 41\,kJ\,mol^{-1}$ in Table 3 suggests that the reason for the sudden decrease in fluorescence quantum yield is photodissociation over the barrier.

CF fragments have been measured following excitation of :CFBr throughout the range as shown in Figure 12. The photofragment excitation (phofex) spectrum, measured by scanning the photolysis laser whilst probing CF, is shown in the lower half of Figure 12. There are a couple of features that appear also in the LIF spectrum, but many additional strong features after the LIF spectrum has died out. The peaks between 24,000 and $24{,}250\,cm^{-1}$ remain sharp, and are clearly assigned from their vibrational spacing and rotational contour analysis as belonging to the same :CFBr progressions as assigned in the LIF spectrum. Even the broadened features near $24{,}500\,cm^{-1}$ can be fit by a lifetime broadened rotational contour from the LIF spectrum [44]. A Lorentzian function has also been used to model the spectral broadening to infer a lifetime of the excited state; several of the lifetimes so derived are shown above peaks in the phofex spectrum. The lifetimes from both LIF and phofex spectra portray a consistent picture of a reaction rate that is increasing rapidly as the energy above the transition state on the $\tilde{A}$ state is increased.

Figure 13 shows CF product rotational state distributions following excitation of :CFBr at two different energies: $T_{00} + 2966\,cm^{-1}$, which is in the region where the transition is visible in both LIF and phofex spectrum, and $T_{00} + 4150\,cm^{-1}$, which lies considerably above the barrier. Excitation well-above the barrier produces an equal

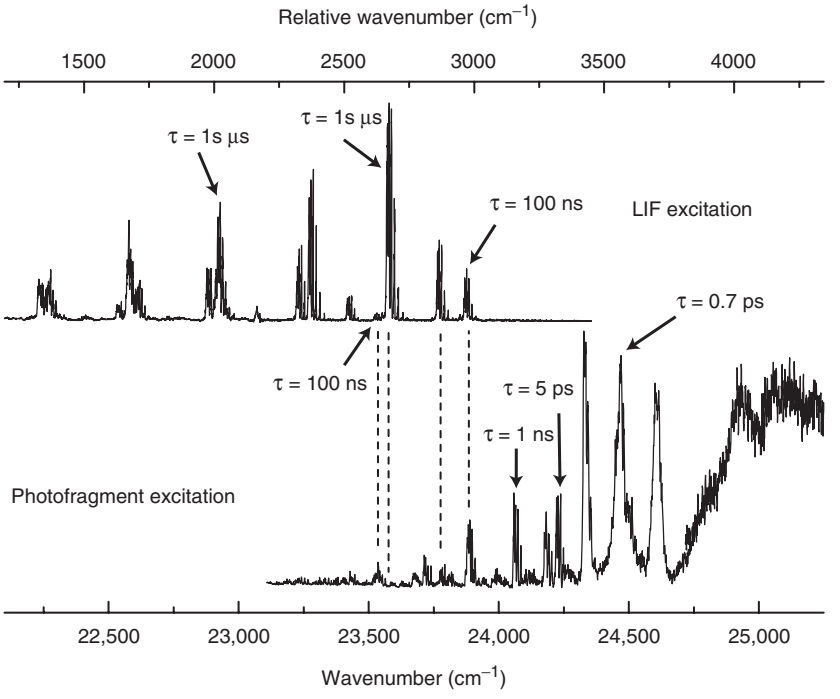

Figure 12. LIF and photofragment excitation spectra of :CFBr. Several transition common in both spectra are indicated by a dashed line. The fluorescence lifetime (upper spectrum) or lifetimes inferred from homogeneous broadening (lower spectrum) are indicated for several peaks.

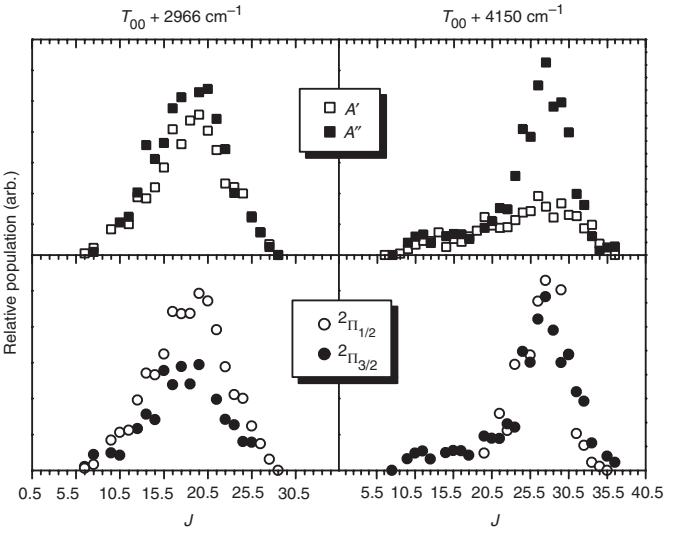

Figure 13. Rotational distributions for the CF photofragment following dissociation of :CFBr at two different energies. At low energy, the $^2\Pi_{1/2}$ state is preferred, while Λ-doublet components are approximately equal. At high energy the A'' Λ-doublet component is preferred while the spin–orbit states are equally populated.

population in the spin–orbit states of the CF ($^2\Pi$) product and a significant enhancement of the A'' lambda doublet state over the A' state. In the high J limit, the A' lambda doublet state corresponds to the unpaired electron lying in the plane of the rotating CF fragment, whereas in the A'' state the electron is perpendicular to the plane. The enhancement of the population in the A'' lambda doublet state of CF reflects fast reaction that preserves the overall A'' electronic symmetry throughout the reaction, from the A'' symmetry of the initial $\tilde{A}$ state through the avoided crossing with the A'' component of the $^2\Pi$ state and through the asymptote of the A'' lambda doublet component of the CF product.

The spin–orbit populations of the CF ($^2\Pi_{1/2}$ and $^2\Pi_{3/2}$) are equally populated at higher energies. (The excited $^2\Pi_{1/2}$ spin–orbit state of the Br co-fragment is energetically inaccessible.) These two states mix thoroughly in the region of the avoided crossing and, after the crossing, the two fragments evolve quickly on the repulsive surface, which preserves the equal population through to final products.

Photodissociation at lower energy produces just the reverse: an approximately equal lambda doublet population distribution, and a preference for the ground state CF ($\tilde{X}\,^2\Pi_{1/2}$). These product state distributions are consistent with a chemical pathway that proceeds without a barrier in the exit channel. Dissociation on a bound PES is well-known to produce a statistical distribution of product states. The preference of the lower energy $^2\Pi_{1/2}$ spin–orbit component in CF over the $^2\Pi_{3/2}$ one simply reflects the statistical preference. The $\tilde{X}$ state of :CFBr correlates with the lowest spin–orbit component of CF, while the triplet $\tilde{a}$ state correlates with both spin–orbit components. The presence of both components in the products, however, is not sufficient to implicate the $\tilde{a}\,^3A''$ over the $\tilde{X}\,^1A'$ state because long-range spin–orbit interactions will mix these two states. The equal population of lambda doublet components also reflects the long-lived, statistical nature of dissociation on a bound PES.

It is interesting also to note that the fluorescence lifetime of states below the barrier is variable. States assigned as combinations of bend (ν_2) and C–Br stretch (ν_3) exhibit lifetimes in the range 2–3 μs. Vibrational states with one or more quanta of CF stretch vibration (ν_1), however, have significantly shorter fluorescence lifetimes: 100–500 ns. The effect of this lifetime shortening shows up dramatically in the phofex spectrum, where peaks with long fluorescence lifetimes appear more weakly in the phofex spectrum than do the peaks with shorter lifetimes. Clearly, excitation of the CF-stretch vibration enhances the curve-crossing to the $\tilde{a}$ or $\tilde{X}$ state from which :CFBr dissociates.

In summary, :CFBr dissociates both directly on the $\tilde{A}$ state surface, via a barrier, as well as on either $\tilde{a}$ and/or $\tilde{X}$ state pathways, which are barrierless. Reaction over the barrier funnels is the reaction through a well-defined part of the PES, from which the A'' lambda doublet population in CF is preferred, while spin–orbit states are equally populated. Below the barrier, the slow dissociation on the bound surface allows mixing of the spin–orbit and lambda doublet states at long range in the exit channel and a statistical distribution of product states.

5.2.2. *CFCl*

The photodissociation of CFCl has also been explored, but only from the viewpoint of spectroscopy; neither the CF nor Cl products of photodissociation have not been measured. However, the LIF spectrum of jet-cooled CFCl shows remarkable similarity to CFBr in most respects. The progressions are longer; nonetheless, they are truncated for

$E_{vib} > T_{00} + 3500\,cm^{-1}$. In the last $500\,cm^{-1}$ of the LIF spectrum, the fluorescence lifetime shortens from 600–700 ns to <15 ns for the last peak. All these spectroscopic indicators imply a photochemistry similar to :CFBr, but confirmation awaits detection of the fragment products.

5.3. *Photochemistry of the $\tilde{B}$ state*

The second excited singlet state, $\tilde{c}\,^1A_1$ in $:CH_2$ or $\tilde{B}$ ($^1A'$ or $^1A_1$) in the halocarbenes has received little attention. Part of the $\tilde{c} \leftarrow \tilde{a}$ transition in $:CH_2$ was actually reported more than 50 years ago [116], however, it was not assigned until very recently [214]. The $\tilde{c} \leftarrow \tilde{a}$ or $\tilde{B} \leftarrow \tilde{X}$:CHX transition although symmetry allowed, is weak because, in a single configuration molecular orbital picture it is formally a two-electron transition. OODR schemes, using two successive one-photon transitions have therefore been employed successfully to prepare the $\tilde{c}$ state of $:CH_2$ [157] and the $\tilde{B}$ state of :CHF [102], :CDF and CHCl (Figure 11) [209]. The Franck–Condon region of the $\tilde{c}$ state in CH_2 lies just below the thermochemical dissociation energy of the C–H bond and the spectroscopic transitions are sharp. Increasing vibrational excitation prepares predissociative states resulting in lifetime broadening of the lines. The $\tilde{B}$ state of the three monohalocarbenes lies above the thermochemical dissociation energy and all OODR lines are broadened. Further, we review the photochemistry of the $\tilde{B}$ state of CHF and CDF in more detail.

5.3.1. *:CHF/ :CDF*

The $\tilde{B}\,^1A'$ state of :CHF is quasilinear and lies about the same energy above the $\tilde{A}$ state that the $\tilde{A}$ state does above the ground state (Figure 14). This almost equal spacing was important in the chance discovery of the OODR $\tilde{X} \rightarrow \tilde{A} \rightarrow \tilde{B}$ spectrum. In a series of experiments designed to probe the $\tilde{a}$ state of CHF by SEP, a series of broadened lines were discovered. In the SEP experiment, a single rovibrational level of the $\tilde{A}$ state is prepared by laser excitation of jet-cooled :CHF. A second laser is scanned through $\tilde{A} \rightarrow \tilde{X}$ resonances. When a resonance is reached, the fluorescence signal is depressed. A measurement of fluorescence suppression as a function of 'dump' wavelength provides an SEP spectrum, which is a 'folded' OODR spectrum. Figure 14 shows several short regions of the OODR spectrum and SEP lines ($\tilde{X} \rightarrow \tilde{A} \rightarrow \tilde{X}$) are indicated with an asterisk. The linewidth of these SEP features is limited by the laser linewidth.

Figure 14 also shows several of the broadened features of the OODR fluorescence depletion experiment that were subsequently assigned as depleting the $\tilde{A}$ state population via the $\tilde{A} \rightarrow \tilde{B}$ transition. The $\tilde{A} \rightarrow \tilde{B}$ spectrum shows all the hallmarks of a classic bent-linear transition, where the K_a states of the bent molecule transforms into vibrational angular momentum states of the linear molecule, labelled by l, and K_c doublet states of the bent molecule become different parity states in the linear molecule. For a full discussion of vibrational and rotational spectroscopic assignments, we refer the reader to the original paper [103].

For the present discussion of the photochemistry we note that the linewidths in the $\tilde{X} \rightarrow \tilde{A} \rightarrow \tilde{B}$ OODR spectrum vary considerably with energy. The Lorentzian linewidths for all vibrational levels assigned as purely bending $(0,v_2{}^l,0)$, as well as states with one quantum of either CH/CD or CF stretch along with bending quanta, i.e. $(1,v_2{}^l,0)$

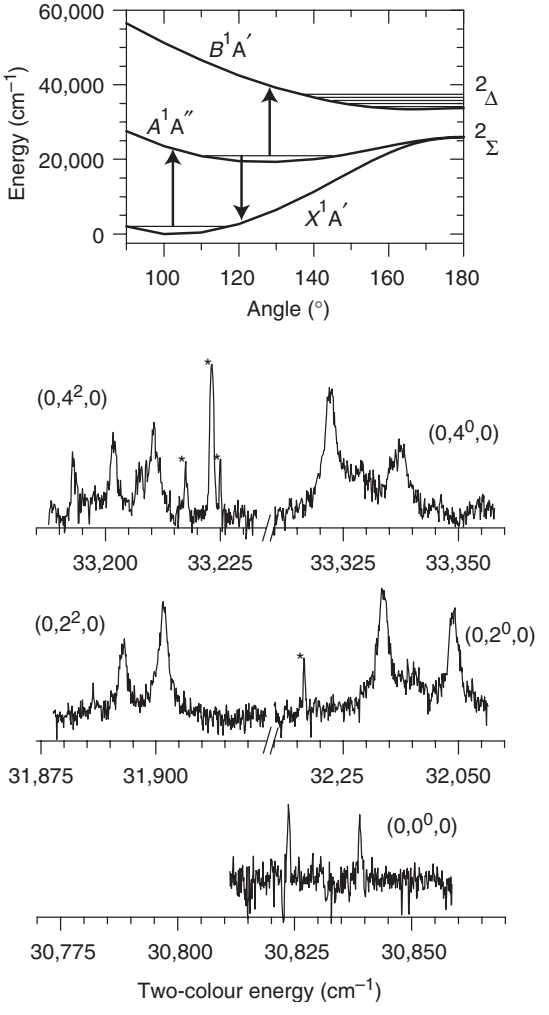

Figure 14. OODR spectra of :CHF showing sharp SEP ($\tilde{X} \rightarrow \tilde{A} \rightarrow \tilde{X}$) lines and broadened 2-photon excitation ($\tilde{X} \rightarrow \tilde{A} \rightarrow \tilde{B}$) lines. The linewidths are broader for higher energy excitation.

or (0,v_2',1), are plotted as a function of vibrational energy for both CDF and CHF in Figure 15. Considering first the CDF data in the upper panel, the linewidth of the purely bending states increases from 0.29 cm^{-1}, at the origin, to about 4 cm^{-1} for the (0,10^l,0) states. This corresponds to a decrease in $\tilde{B}$ state lifetime from one of the order of 10 ps at the zero-point level, to approximately 1 ps at the energy of 10 quanta of bend. Addition of one quantum of CD or CF stretch does not do vary much to the lifetime; bend-stretch combination states have similar linewidths to the pure bending states for the same energy. The linewidths of the pure bending states in the CHF OODR spectrum (lower panel of Figure 15) are slightly broader than CDF, though, overall, a largely similar behaviour is observed. Addition of one quantum of CH stretch does not change this behaviour;

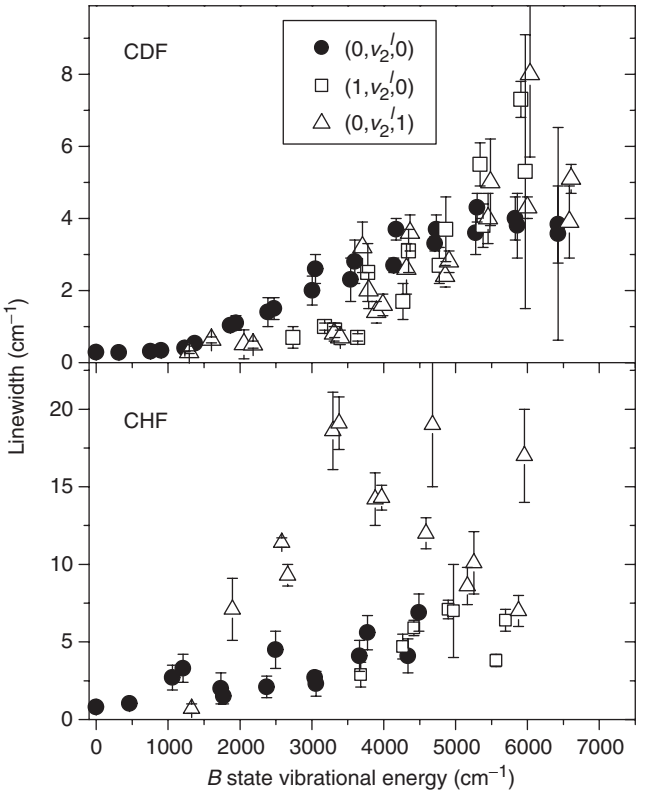

Figure 15. Homogeneous linewidths for many vibrational states in the OODR ($\tilde{X} \rightarrow \tilde{A} \rightarrow \tilde{B}$) spectrum of :CDF and :CHF. In :CDF the linewidths increase more-or-less monotonically with increased energy, while in :CHF, excitation of the CF-stretch (ν_3) enhances the predissociation rate.

however, addition of one quantum of CF stretch results in much broader lines – up to $20\,\mathrm{cm}^{-1}$, corresponding to a $\tilde{B}$ state lifetime of $\sim$200 fs.

The mechanism of the lifetime shortening, whilst almost certainly due to dissociation, is not clear. Not only is the dissociative state unclear, but the actual chemical products have not been identified. At this energy in CDF and CHF there are two chemical reaction channels open:

$$\mathrm{CHF/CDF}(\tilde{B}^1A') \rightarrow \mathrm{CF}(^2\Pi) + \mathrm{H/D}$$

$$\text{or} \quad \mathrm{CHF/CDF}(\tilde{B}^1A') \rightarrow \mathrm{C}(^3P) + \mathrm{HF/DF}$$

The $\mathrm{C}(^3P)$ pathway, which actually produces the lower energy products, correlates with the A'' state of CHF/CDF. Preliminary *ab initio* calculations reveal that the $\mathrm{C}(^3P)$ channel proceeds over a significant barrier, which is exceeded at these energies. The simple bond cleavage pathway correlates with $\tilde{X}$, $\tilde{a}$ and $\tilde{A}$ states, as discussed earlier, and, whilst at higher energy, proceeds without a barrier on the $\tilde{X}$ and $\tilde{a}$ states. There will also be a number of other repulsive states that cross the $\tilde{B}$ state as indicated in Figure 10. The origin of the mode-specific lifetime shortening for bend-stretch combination states in CHF is also

unknown. Possibilities include crossing to a second electronic surface, or an enhancement of the rate on the same surface.

5.4. *Photochemistry beyond the $\tilde{B}$ state*

There have been experimental studies on photodissociation of a number of halocarbenes at higher energy, including :CCl_2, :CHCl, :CFCl and :CFBr. The most extensively explored molecule is :CCl_2 which has been dissociated at 308, 248 and 193 nm by three different groups using different techniques [46–48,211,215]. The carbenes :CHCl [210], CFCl [45] and CFBr [45] have also been studied at a photolysis wavelength of 193 nm. While calculations have been reported for the energy and structure of the $\tilde{X}$, $\tilde{a}$ and $\tilde{A}$ states of essentially all halocarbenes, to our knowledge, calculations of electronic states corresponding to these energies, particularly the higher lying Rydberg states, have been carried out only for :CF_2 [170] and :CCl_2 [175].

5.4.1. *Photodissociation of :CCl_2 at 248 nm*

Excitation of dichloromethylene at 248 nm provides energy of 482 kJ mol^{-1}, which, according to the threshold in Table 3, is 163 kJ mol^{-1} above that required to break the C–Cl bond. The photofragment translational spectra of both CCl and Cl fragments have been measured. The centre-of-mass kinetic energy distribution derived from these measurements is shown in Figure 16. The distribution is rather triangular, peaking at 100 kJ mol^{-1} and extending asymmetrically from almost zero to nearly to the limit of available energy (note that the available energy in the original paper is ~100 kJ mol^{-1} higher due to use of a different reaction enthalpy to that in Table 3).

The CCl product rotational distribution at 248 nm excitation has also been deduced from measurement of the nascent CCl $\tilde{A} \leftarrow \tilde{X}$ LIF spectrum [46,48]. The rotational distribution, with F_1 and F_2 components averaged, is also reproduced in Figure 16, and shows two clear components – one centred near $J = 85$, and the other near $J = 10$. The average CCl rotational energy associated with each component is 62 and 1.5 kJ mol^{-1}, respectively. Very little vibrational excitation of the CCl was reported in the LIF spectrum, although it was noted that the measurement of excited vibrational states of CCl is difficult because the Franck–Condon factors are very diagonal, and excited vibrational levels in the $\tilde{A}$ state are predissociated. The ratio of the two components was shown to vary with the mole fraction of the precursor $CHCl_3$ in the flash pyrolysis nozzle that was used to generate :CCl_2 [46]. The higher J component increased in dominance for lower mole fraction. Kinetic modelling of the flash pyrolysis conditions indicated that not only the primary $CHCl_3$ pyrolysis channel produces :CCl_2 + HCl, but that secondary reactions can also produce CCl_3. The importance of these secondary, bimolecular, reactions increased with increasing the mole fraction of $CHCl_3$. It seems apparent that the high J part of the rotational distribution can be attributed clearly to photodissociation of :CCl_2. At least part of the low J distribution results from photodissociation of CCl_3. However, the low J component did not diminish as rapidly as did the CCl_3 concentration in kinetic modelling and so the authors concluded that there might be two different mechanisms in the 248 nm dissociation of :CCl_2.

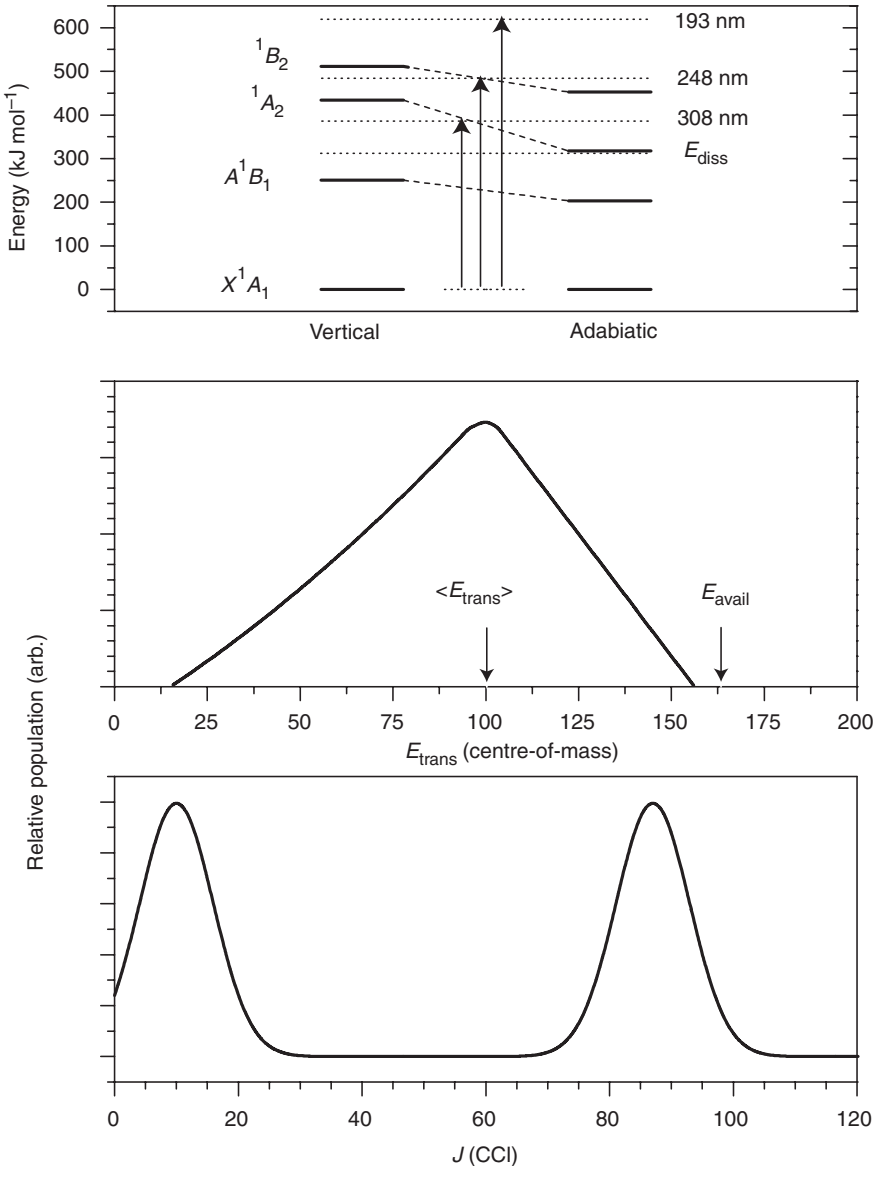

Figure 16. Summary of experimental measurements of the 248 nm photodissociation of :CCl_2 and theoretical calculations of vertical and adiabatic excitation energies for the lowest :CCl_2 electronic states of each symmetry [175]. The rotational distribution, from Ref. [48] is the average of the F_1 and F_2 components at low backing pressure, while the translational energy graph is adapted from Figure 2 in Ref. [211].

The high J rotational component correlates very well with the translational energy distribution: $\langle E_{trans} \rangle = 100\,kJ\,mol^{-1}$ plus $\langle E_{rot} \rangle = 62\,kJ\,mol^{-1}$ is in excellent agreement with the total available energy of $168\,kJ\,mol^{-1}$. It seems likely that the high J rotational distribution and the translational energy measurements correspond to the same

photodissociation mechanism. If the low J component also arises from dissociation of :CCl_2 then this must involve another mechanism – most likely a different electronic state.

Figure 16 summarises the calculated vertical and adiabatic excitation energies for the lowest energy electronic state of CCl_2 in each symmetry species [175]. This set of states is not complete within this energy range. In particular, we note that the pseudo-linear $\tilde{B}\ ^1A_1$ state, referred to in the previous section is not included; it has the same symmetry as the ground state and is therefore much more difficult to calculate. Transitions between the ground states A_1 and $^1A_2$ are dipole forbidden, while the $^1B_2 \leftarrow \tilde{X}$ transition was calculated to be about seven times stronger than the $\tilde{A} \leftarrow \tilde{X}$ transition. The missing $\tilde{B} \leftarrow \tilde{X}$ transition, although symmetry allowed, is a two electron transition, and therefore expected to be much weaker than the $^1B_2 \leftarrow \tilde{X}$. Both Morley *et al*. [211] and Shin and Dagdigian [46] have therefore assigned the transition at 248 nm to $^1B_2 \leftarrow \tilde{X}$. The mechanism favoured by both groups is that the $^1B_2$ state crosses with a dissociative state correlating with ground state products. The highly bent nature of the $^1B_2$ state, and the kinematic combination of 'heavy–light–heavy' atoms in :CCl_2 then ensure that a large fraction of the excess energy is partitioned into rotational motion of the diatomic fragment.

5.4.2. *Photodissociation of halocarbenes at 193 nm*

Photodissociation of four halocarbenes: :CCl_2, :CHCl, :CFCl and :CFBr, following 193 nm excitation, has been explored by Shin and Dagdigian [45,47,210]. Absorption of a 193 nm photon in each case was assigned to excitation of a Rydberg state. In all cases, measurement of the LIF spectrum of the diatomic fragment showed that the reaction produces relatively modest rotational or vibrational excitation; the average rotational energy of the diatomic fragment was 7.5% for :CHCl, 5% for :CCl_2, 2% for :CFCl and 1.5% for :CFBr. The first excited state of the diatomic fragment remains inaccessible at this energy and so most of the available energy must be partitioned into relative translational motion of the fragments. Indeed, the rotational lines in the CF LIF spectrum were significantly Doppler broadened, consistent with this conclusion.

The results of all four experiments at 193 nm are fairly similar and it seems likely that the same photochemical mechanism is responsible in each case. The authors suggest that a linear state of the halocarbene must be involved to generate such low-rotational excitation of the diatomic fragment. This might be the pseudo-linear $\tilde{B}$ (A' or $^1A_1$) state, however, there are numerous other states lying in the region of a 193 nm photon, especially when repulsive and spin–orbit states are included.

6. Summary and conclusions

In this review we have attempted to show that the halocarbenes are model systems for understanding the complicated spectroscopy, photochemistry and photophysics of carbenes, as well as benchmarks for comparing experiment and theory for carbene singlet–triplet gaps. Although the halocarbenes have been studied for almost 50 years, only in the last decade has real progress been made on many of these fronts, and we are confident that in the coming years new experimental and theoretical techniques will continue to shed light on these important reactive intermediates. We have stressed the synergy between

experiment and theory that permeates the history of carbene chemistry, and we have no doubt this will continue.

Future work will no doubt focus on the photochemistry and photodissociation dynamics of the halocarbenes, with the possibility of detecting the $\tilde{B}$ state in other halocarbenes. As noted also in their spectroscopy, the photodissociation dynamics of even the simplest carbenes are quite complicated because of the number of interacting electronic states at the energy required for dissociation, and we can anticipate that a combination of experiment and new theoretical methods will be brought to bear on this important problem. As we have noted, the recent application of time-resolved photoionisation and photoelectron methods is an exciting development in the study of carbene spectroscopy and dynamics, which we are sure will continue to be explored.

References

[1] W. von E. Doering, R. G. Buttery, R. G. Laughlin, and N. Chaudhuri, J. Am. Chem. Soc. **78**, 3224 (1956).
[2] D. B. Richardson, M. C. Simmons, and I. Dvoretzky, J. Am. Chem. Soc. **82**, 5001 (1990).
[3] R. A. Moss, M. S. Platz, and M. Jones Jr., editors, *Reactive Intermediate Chemistry* (Wiley-Interscience, Hoboken, NJ, 2004).
[4] H. F. Schaefer III, Science **231**, 1100 (1986).
[5] J. M. Foster and S. F. Boys, Rev. Mod. Phys. **32**, 305 (1960).
[6] G. Herzberg, Proc. R. Soc. London Ser. A **262**, 291 (1961).
[7] P. C. H. Jordan and H. C. Longuet-Higgins, Mol. Phys. **5**, 121 (1962).
[8] J. A. Pople and G. A. Segal, J. Chem. Phys. **44**, 3289 (1966).
[9] J. F. Harrison and L. C. Allen, J. Am. Chem. Soc. **91**, 807 (1969).
[10] C. F. Bender and H. F. Schaefer III, J. Am. Chem. Soc. **92**, 4984 (1970).
[11] R. A. Benheim, H. W. Bernard, P. S. Wang, L. S. Wood, and P. S. Skell, J. Chem. Phys. **53**, 1280 (1970).
[12] R. A. Benheim, H. W. Bernard, P. S. Wang, L. S. Wood, and P. S. Skell, J. Chem. Phys. **54**, 3223 (1971).
[13] E. Wasserman, V. J. Kuck, R. S. Hutton, and W. A. Yager, Chem. Phys. Lett. **7**, 409 (1970).
[14] J. Hine, J. Am. Chem. Soc. **72**, 2438 (1950).
[15] W. von E. Doering and A. K. Hoffmann, J. Am. Chem. Soc. **76**, 6162 (1954).
[16] W. von E. Doering and W. A. Henderson Jr., J. Am. Chem. Soc. **80**, 5274 (1958).
[17] L. D. Wescott and P. S. Skell, J. Am. Chem. Soc. **87**, 1721 (1965).
[18] P. S. Skell and A. Y. Gardner, J. Am. Chem. Soc. **78**, 5430 (1956).
[19] W. von E. Doering and W. A. Henderson Jr., J. Am. Chem. Soc. **80**, 5274 (1958).
[20] P. Venkateswarlu, Phys. Rev. **77**, 676 (1950).
[21] R. K. Laird, E. B. Andrews, and R. F. Barrow, Trans. Faraday Soc. **46**, 803 (1950).
[22] D. E. Mann and B. A. Thrush, J. Chem. Phys. **33**, 1732 (1960).
[23] A. M. Bass and D. E. Mann, J. Chem. Phys. **36**, 3501 (1962).
[24] B. A. Thrush and J. J. Zwolenik, Trans. Faraday Soc. **59**, 582 (1963).
[25] A. J. Merer and D. N. Travis, Can. J. Phys. **44**, 525 (1966).
[26] A. J. Merer and D. N. Travis, Can. J. Phys. **44**, 1541 (1966).
[27] H. Staudinger and R. Endle, Chem. Ber. **46**, 1437 (1913).
[28] L. P. Blanchard and P. Le Goff, Can. J. Chem. **35**, 89 (1957).
[29] W. I. Bevan, R. N. Haszeldine, and J. C. Young, Chem. Ind. 789 (1961).
[30] J. S. Shapiro and F. P. Lossing, J. Phys. Chem. **72**, 1552 (1968).

[31] P. S. Skell and M. S. Cholod, J. Am. Chem. Soc. **91**, 6035 (1969).
[32] M. B. Knickelbein, D. A. Webb, and E. R. Grant, Mat. Res. Soc. Sym. Proc. **38**, 23 (1985).
[33] P. Chen, S. D. Colson, W. A. Chupka, and J. A. Berson, J. Phys. Chem. **90**, 2319 (1986).
[34] D. W. Kohn, H. Clauberg, and P. Chen, Rev. Sci. Instrum. **63**, 4003 (1992).
[35] J. A. Blush, H. Clauberg, D. W. Kohn, D. W. Minsek, X. Zhang, and P. Chen, Acc. Chem. Res. **25**, 385 (1992).
[36] D. J. Clouthier and J. Karolczak, J. Phys. Chem. **93**, 7542 (1989).
[37] D. J. Clouthier and J. Karolczak, J. Chem. Phys. **94**, 1 (1991).
[38] J. I. Choe, S. R. Tanner, and M. D. Harmony, J. Mol. Spectr. **138**, 319 (1989).
[39] D. W. Kohn, E. S. J. Robles, C. F. Logan, and P. Chen, J. Phys. Chem. **97**, 4936 (1993).
[40] T. Pancur, K. Brendel, N. Hansen, H. Maeder, V. Markov, and F. Temps, J. Mol. Spectrosc. **232**, 375 (2005).
[41] M. R. Cameron and S. H. Kable, Rev. Sci. Instrum. **67**, 283 (1996).
[42] M. R. Cameron, S. H. Kable, and G. B. Bacskay, J. Chem. Phys. **103**, 4476 (1995).
[43] P. T. Knepp, C. K. Scalley, G. B. Bacskay, and S. H. Kable, J. Chem. Phys. **109**, 2220 (1998).
[44] P. T. Knepp and S. H. Kable, J. Chem. Phys. **110**, 11789 (1999).
[45] S. K. Shin and P. J. Dagdigian, J. Chem. Phys. **126**, 134302 (2007).
[46] S. K. Shin and P. J. Dagdigian, J. Chem. Phys. **128**, 154322 (2008).
[47] S. K. Shin and P. J. Dagdigian, J. Chem. Phys. **125**, 133317 (2006).
[48] S. K. Shin and P. J. Dagdigian, Phys. Chem. Chem. Phys. **8**, 3446 (2006).
[49] G. L. Closs and J. J. Coyle, J. Am. Chem. Soc. **84**, 4350 (1962).
[50] N. J. Turro, J. A. Butcher Jr., R. A. Moss, W. Guo, R. C. Munjal, and M. Fedorynski, J. Am. Chem. Soc. **102**, 7576 (1980).
[51] L. J. Schoen and D. E. Mann, J. Chem. Phys. **41**, 1514 (1964).
[52] D. E. Milligan, D. E. Mann, M. E. Jacox, and R. A. Mitsch, J. Chem. Phys. **41**, 1199 (1964).
[53] F. W. Dalby, J. Chem. Phys. **41**, 2297 (1964).
[54] C. W. Mathews, J. Chem. Phys. **45**, 1068 (1966).
[55] M. E. Jacox and D. E. Milligan, J. Chem. Phys. **50**, 3252 (1969).
[56] M. Robert, J. P. Toscano, M. S. Platz, S. C. Abbot, M. M. Kirchhoff, and R. P. Johnson, J. Phys. Chem. **100**, 18426 (1996).
[57] J. S. Guss, O. Votava, and S. H. Kable, J. Chem. Phys. **115**, 11118 (2001).
[58] R. I. Martinez and J. T. Herron, Chem. Phys. Lett. **84**, 180 (1981).
[59] A. Ortiz de Zarate, R. Martinez, M. N. Sanchez Rayo, F. Castano, and G. Hancock, J. Chem. Soc. Faraday Trans. **88**, 535 (1992).
[60] G. Hancock and G. W. Ketley, J. Chem. Soc. Faraday Trans. **78**, 1283 (1982).
[61] M. N. R. Ashfold, F. Castano, G. Hancock, and G. W. Ketley, Chem. Phys. Lett. **73**, 421 (1980).
[62] R. Steudel, Tetrahed. Lett. **19**, 1845 (1967).
[63] B. M. Dobrynin, V. B. Kislyakov, and V. G. Maslennikov, Z. Tech. Fiziki **49**, 2516 (1979).
[64] R. Schlachta, G. Lask, S. H. Tsay, and V. E. Bondybey, Chem. Phys. **155**, 267 (1991).
[65] R. Schlachta, G. M. Lask, and V. E. Bondybey, J. Chem. Soc. Faraday Trans. **87**, 2407 (1991).
[66] R. Schlachta, G. Lask, A. Stangassinger, and V. E. Bondybey, J. Phys. Chem. **95**, 7132 (1991).
[67] A. Thoma, B. E. Wurfel, R. Schlachta, G. M. Lask, and V. E. Bondybey, J. Phys. Chem. **96**, 7231 (1992).
[68] M. Kakimoto, S. Saito, and E. Hirota, J. Molec. Spectrosc. **97**, 194 (1983).
[69] J. Bloch, R. W. Field, G. E. Hall, and T. J. Sears, J. Chem. Phys. **101**, 1717 (1994).
[70] Z. Wang, R. G. Bird, H.-G. Yu, and T. J. Sears, J. Chem. Phys. **124**, 074314 (2006).
[71] A. Lin, K. Kobayashi, H.-G. Yu, G. E. Hall, J. T. Muckerman, T. J. Sears, and A. J. Merer, J. Mol. Spectr. **214**, 216 (2002).
[72] A. J. Marr and T. J. Sears, Molec. Phys. **99**, 185 (1999).
[73] B.-C. Chang and T. J. Sears, J. Chem. Phys. **102**, 6347 (1995).
[74] B.-C. Chang and T. J. Sears, J. Mol. Spectr. **173**, 391 (1995).

[75] B.-C. Chang and T. J. Sears, J. Chem. Phys. **105**, 2135 (1996).
[76] B.-C. Chang, R. Fei, and T. J. Sears, J. Mol. Spectr. **183**, 341 (1997).
[77] A. J. Marr, S. W. North, T. J. Sears, L. Ruslen, and R. W. Field, J. Mol. Spectr. **188**, 68 (1998).
[78] H.-G. Yu, T. Gonzalez-Lezana, A. J. Marr, J. T. Muckerman, and T. J. Sears, J. Chem. Phys. **115**, 5433 (2001).
[79] B.-C. Chang, J. S. Guss, and T. J. Sears, J. Mol. Spectr. **219**, 136 (2003).
[80] T. W. Schmidt, G. B. Bacskay, and S. H. Kable, J. Chem. Phys. **110**, 11277 (1999).
[81] R. J. Butcher, S. Saito, and E. Hirota, J. Chem. Phys. **80**, 4000 (1984).
[82] T. Suzuki, S. Saito, and E. Hirota, Can. J. Phys. **62**, 1328 (1984).
[83] T. Suzuki and E. Hirota, J. Chem. Phys. **85**, 5541 (1986).
[84] R. N. Dixon and N. G. Wright, Chem. Phys. Lett. **100**, 311 (1983).
[85] K. Hakuta, J. Mol. Spectr. **106**, 56 (1984).
[86] H. Fan, I. Ionescu, C. Annesley, and S. A. Reid, Chem. Phys. Lett. **378**, 548 (2003).
[87] H. Fan, I. Ionescu, C. Annesley, J. Cummins, M. Bowers, and S. A. Reid, J. Mol. Spectr. **225**, 43 (2004).
[88] I. Ionescu, H. Fan, C. Annesley, J. Xin, and S. A. Reid, J. Chem. Phys. **120**, 1164 (2004).
[89] H. Fan, I. Ionescu, J. Xin, and S. A. Reid, J. Chem. Phys. **121**, 8869 (2004).
[90] I. Ionescu, H. Fan, E. Ionescu, and S. A. Reid, J. Chem. Phys. **121**, 8874 (2004).
[91] H. Fan, I. Ionescu, C. Annesley, J. Cummins, M. Bowers, J. Xin, and S. A. Reid, J. Phys. Chem. A **108**, 3732 (2004).
[92] H. Fan, C. Mukarakate, M. Deselnicu, C. Tao, and S. A. Reid, J. Chem. Phys. **123**, 014314 (2005).
[93] E. Ionescu and S. A. Reid, J. Mol. Struct. THEOCHEM **725**, 45 (2005).
[94] C. Mukarakate, Y. Mishchenko, D. Brusse, C. Tao, and S. A. Reid, Phys. Chem. Chem. Phys. **8**, 4320 (2006).
[95] M. Deselnicu, C. Tao, C. Mukarakate, and S. A. Reid, J. Chem. Phys. **124**, 134302 (2006).
[96] C. Tao, M. Deselnicu, C. Mukarakate, and S. A. Reid, J. Chem. Phys. **125**, 094305 (2006).
[97] C. Tao, C. Mukarakate, and S. A. Reid, J. Chem. Phys. **124**, 224314 (2006).
[98] C. Tao, M. Deselnicu, H. Fan, C. Mukarakate, I. Ionescu, and S. A. Reid, Phys. Chem. Chem. Phys. **8**, 707 (2006).
[99] C. Tao, C. Mukarakate, and S. A. Reid, J. Mol. Spectr. **241**, 136 (2007).
[100] C. Tao, C. Mukarakate, D. Brusse, Y. Mishchenko, and S. A. Reid, J. Mol. Spectr. **241**, 180 (2007).
[101] C. Tao, C. Mukarakate, and S. A. Reid, J. Mol. Spectr. **246**, 113 (2007).
[102] C. Tao, C. Mukarakate, and S. A. Reid, J. Mol. Spectr. **241**, 143 (2007).
[103] C. Tao, S. A. Reid, T. W. Schmidt, and S. H. Kable, J. Chem. Phys. **126**, 051105 (2007).
[104] C. A. Richmond, C. Tao, C. Mukarakate, H. Fan, K. Nauta, T. W. Schmidt, S. H. Kable, and S. A. Reid, J. Phys. Chem. A **112**, 11355 (2008).
[105] C. Tao, C. Mukarakate, R. H. Judge, and S. A. Reid, J. Chem. Phys. **128**, 171101 (2008).
[106] C. Tao, C. Mukarakate, Z. Terranova, C. Ebban, R. H. Judge, and S. A. Reid, J. Chem. Phys. **129**, 104309 (2008).
[107] C. Mukarakate, C. Tao, C. D. Jordan, W. F. Polik, and S. A. Reid, J. Phys. Chem. A **112**, 466 (2008).
[108] C. Tao, C. Ebban, H.-T. Ko, and S. A. Reid, Phys. Chem. Chem. Phys. **10**, 6090 (2008).
[109] T. W. Schmidt, G. B. Bacskay, and S. H. Kable, Chem. Phys. Lett. **292**, 80 (1998).
[110] K. Nauta, J. S. Guss, N. L. Owens, and S. H. Kable, J. Chem. Phys. **120**, 3517 (2004).
[111] C. A. Richmond, J. S. Guss, K. Nauta, and S. H. Kable, J. Mol. Spectr. **231**, 96 (2005).
[112] J. S. Guss, C. A. Richmond, K. Nauta, and S. H. Kable, Phys. Chem. Chem. Phys. **7**, 100 (2005).
[113] Y. Qiu, S. Zhou, and J. Shi, Chem. Phys. Lett. **136**, 93 (1987).
[114] K. K. Irikura, J. W. Hudgens, and R. D. Johnson III, J. Chem. Phys. **103**, 1303 (1995).

[115] B. Noller, L. Poisson, R. Maksimenka, I. Fischer, and J.-M. Mestdagh, J. Am. Chem. Soc. **130**, 14908 (2008).
[116] G. Herzberg and J. W. C. Johns, Proc. Roy. Soc. Lond. Ser. A. **295**, 107 (1966).
[117] A. D. Walsh, J. Chem. Soc. 2288 (1953).
[118] G. E. Hall, T. J. Sears, and H.-G. Yu, J. Mol. Spectr. **235**, 125 (2006).
[119] Z. Wang, Y. Kim, G. E. Hall, and T. J. Sears, J. Phys. Chem. A. **112**, 9248 (2008).
[120] R. Renner, Z. Phys. **92**, 172 (1934).
[121] G. Herzberg, *Electronic Spectra and Electronic Structure of Ployatomic Molecules* (Van Nostrand-Reinhold, New York, 1966).
[122] C. Jungen and A. J. Merer, in *Molecular Spectroscopy: Modern Research*, edited by K. N. Rao (Academic Press, New York, 1976), Vol. 2, pp. 127–164.
[123] C. Jungen and A. J. Merer, Molec. Phys. **40**, 1 (1980).
[124] J. M. Brown and F. Jorgensen, in *Advances in Chemical Physics*, edited by I. Prigogine and S. A. Rice (Wiley, New York, 1983), Vol. 52, pp. 117–180.
[125] G. Duxbury and C. Jungen, Mol. Phys. **63**, 981 (1988).
[126] G. Duxbury, B. D. McDonald, and A. Alijah, Molec. Phys. **89**, 767 (1996).
[127] G. Duxbury and R. N. Dixon, Molec. Phys. **43**, 255 (1981).
[128] P. R. Bunker and P. Jensen, *Molecular Symmetry and Spectroscopy*, 2nd ed (National Research Council of Canada Press, Ottawa, 1998).
[129] H.-G. Yu, J. T. Muckerman, and T. J. Sears, J. Chem. Phys. **116**, 1435 (2002).
[130] M. E. Jacox and D. E. Milligan, J. Chem. Phys. **50**, 3252 (1969).
[131] M. Kakimoto, S. Saito, and E. Hirota, J. Molec. Spectrosc. **88**, 300 (1981).
[132] T. Suzuki and E. Hirota, J. Chem. Phys. **88**, 6778 (1988).
[133] R. I. Patel, G. W. Stewart, K. Caslton, J. G. Gole, and J. R. Lombardi, Chem. Phys. **52**, 461 (1980).
[134] J. M. Brown and A. Carrington, *Rotational Spectroscopy of Diatomic Molecules* (Cambridge University Press, Cambridge, 2003).
[135] E. Hirota, *High Resolution Spectroscopy of Transient Species* (Springer-Verlag, New York, 1985).
[136] R. N. Dixon, Trans. Faraday Soc. **60**, 1363 (1964).
[137] J. T. Hougen and J.K.W.G. Watson, Can. J. Phys. **43**, 298 (1965).
[138] M. Jacox and D. E. Milligan, J. Chem. Phys. **47**, 1626 (1967).
[139] S. Xu, K. A. Beran, and M. D. Harmony, J. Phys. Chem. **98**, 2742 (1994).
[140] C.-W. Chen, T.-C. Tsai, and B.-C. Chang, Chem. Phys. Letts. **347**, 73 (2001).
[141] C.-L. Lee, M.-L. Liu, and B.-C. Chang, J. Chem. Phys. **117**, 3263 (2002).
[142] C.-S. Lin, Y.-E. Chen, and B.-C. Chang, J. Chem. Phys. **121**, 4164 (2004).
[143] G. Tarczay, T. A. Miller, G. Czako, and A. G. Csaszar, Phys. Chem. Chem. Phys. **7**, 2881 (2005).
[144] H.-G. Yu, T. J. Sears, and J. T. Muckerman, Mol. Phys. **104**, 47 (2006).
[145] M. K. Gilles, K. M. Ervin, J. Ho, and W. C. Lineberger, J. Phys. Chem. **96**, 1130 (1992).
[146] T.-S. Tsai, C.-W. Chen, and B.-C. Chang, J. Chem. Phys. **115**, 766 (2001).
[147] C.-W. Chen, T.-C. Tsai, and B.-C. Chang, J. Mol. Spectr. **209**, 254 (2001).
[148] C.-L. Lee, M.-L. Liu, and B.-C. Chang, Phys. Chem. Chem. Phys. **5**, 3859 (2003).
[149] R. E. Huie, N. J. T. Long, and B. A. Thrush, Chem. Phys. Lett. **51**, 197 (1977).
[150] S. Xu and M. D. Harmony, J. Phys. Chem. **97**, 7465 (1993).
[151] H.-J. Hsu, W.-Z. Chang, and B.-C. Chang, Phys. Chem. Chem. Phys. **7**, 2468 (2005).
[152] C. Tao, C. Mukarakate, D. Brusse, Y. Mishchenko, and S. A. Reid, J. Molec. Spectrosc. **240**, 139 (2006).
[153] K. Sendt and G. B. Bacskay, J. Chem. Phys. **112**, 2227 (2000).
[154] B. S. Truscott, N. L. Elliott, and C. M. Western, J. Chem. Phys. **130**, 234301 (2009).
[155] A. R. W. McKellar, P. R. Bunker, T. J. Sears, K. M. Evenson, R. J. Saykally, and S. R. Langhoff, J. Chem. Phys. **79**, 5251 (1983).

[156] C. G. Stevens and J. C. D. Brand, J. Chem. Phys. **58**, 3324 (1973).
[157] Y. Kim, G. E. Hall, and T. J. Sears, J. Mol. Spectr. **240**, 269 (2006).
[158] Z. Wang, Y. Kim, G. E. Hall, and T. J. Sears, J. Phys. Chem. A. **112**, 9248 (2008).
[159] J. F. Harrison, J. Am. Chem. Soc. **93**, 4112 (1971).
[160] V. Staemmler, Theor. Chim. Acta **35**, 309 (1974).
[161] T. Takabe, M. Takahashi, and H. Fukutome, Prog. Theor. Phys. **56**, 689 (1976).
[162] C. W. Bauschlicher Jr., H. F. Schaefer Jr., and P. S. Bagus, J. Am. Chem. Soc. **99**, 7106 (1977).
[163] N. C. Baird and K. F. Taylor, J. Am. Chem. Soc. **100**, 1333 (1978).
[164] P. H. Mueller, N. G. Rondan, K. N. Houk, J. F. Harrison, D. Hooper, B. H. Willen, and J. F. Liebman, J. Am. Chem. Soc. **103**, 5049 (1981).
[165] G. E. Scuseria, M. Duran, R.G.A.R. Maclagan, and H. F. Schaefer III, J. Am. Chem. Soc. **108**, 3248 (1986).
[166] E. A. Carter and W. A. Goddard III, J. Phys. Chem. **91**, 4651 (1987).
[167] E. A. Carter and W. A. Goddard III, J. Chem. Phys. **88**, 1752 (1988).
[168] S. K. Shin, W. A. Goddard III, and J. L. Beauchamp, J. Phys. Chem. **94**, 6963 (1990).
[169] K. K. Irikura, W. A. Goddard III, and J. L. Beauchamp, J. Am. Chem. Soc. **114**, 48 (1992).
[170] R. Vetter, W. Reuter, and S. D. Peyerimhoff, Chem. Phys. **161**, 379 (1992).
[171] N. Russo, E. Sicilia, and M. Toscano, J. Chem. Phys. **97**, 5031 (1992).
[172] A. Gobbi and G. Frenking, Bull. Chem. Soc. Jpn. **66**, 3153 (1993).
[173] A. Gobbi and G. Frenking, J. Chem. Soc. Chem. Commun. **14**, 1162 (1993).
[174] N. Russo, E. Sicilia, and M. Toscano, Chem. Phys. Lett. **213**, 245 (1993).
[175] Z. L. Cai, J. Phys. Chem. **97**, 8399 (1993).
[176] V. M. Garcia, O. Castell, M. Reguero, and R. Caballol, Mol. Phys. **87**, 1395 (1996).
[177] S. E. Worthington and C. J. Cramer, J. Phys. Org. Chem. **10**, 755 (1997).
[178] J. C. Poutsma, J. A. Paulino, and R. R. Squires, J. Phys. Chem. A **101**, 5327 (1997).
[179] R. Vargas, M. Galvan, and A. Vela, J. Phys. Chem. A **102**, 3134 (1998).
[180] Z. Havlas and J. Michl, Coll. Czech. Chem. Com. **63**, 1485 (1998).
[181] M. Schwartz and P. Marshall, J. Phys. Chem. A **103**, 7900 (1999).
[182] D. Das and S. L. Whittenburg, THEOCHEM **492**, 175 (1999).
[183] F. Mendez and M. A. Garcia-Garibay, J. Org. Chem. **64**, 7061 (1999).
[184] C.-H. Hu, Chem. Phys. Lett. **309**, 81 (1999).
[185] B. Hajgato, H. M. T. Nguyen, T. Veszpremi, and M. T. Nguyen, Phys. Chem. Chem. Phys. **2**, 5041 (2000).
[186] K. Sendt, T. W. Schmidt, and G. B. Bacskay, Int. J. Quant. Chem. **76**, 297 (2000).
[187] A. P. Scott, M. S. Platz, and L. Radom, J. Am. Chem. Soc. **123**, 6069 (2001).
[188] L. V. Slipchenko and A. I. Krylov, J. Chem. Phys. **117**, 4694 (2002).
[189] A. Kalemos, T. H. Dunning, A. Mavridis, and J. F. Harrison, Can. J. Chem. **82**, 684 (2004).
[190] J. Olah, F. De Proft, T. Veszpremi, and P. Geerlings, J. Phys. Chem. A **108**, 490 (2004).
[191] J. S. Guss, G. B. Bacskay, and S. H. Kable, Chem. Phys. Lett. **405**, 258 (2005).
[192] F.-t. Chau, D. K. W. Mok, E. P. F. Lee, and J. M. Dyke, Chem. Phys. Chem. **6**, 2037 (2005).
[193] M. L. McKee and J. Michl, J. Phys. Chem. A **106**, 8495 (2002).
[194] T. Ha, H. U. Gremlich, and R. E. Buhler, Chem. Phys. Lett. **65**, 16 (1979).
[195] G. L. Gutsev and T. Ziegler, J. Phys. Chem. **95**, 7220 (1991).
[196] J. M. Dyke, E. P. F. Lee, D. K. W. Mok, and F.-T. Chau, Chem. Phys. Chem. **6**, 2046 (2005).
[197] K. K. Murray, D. G. Leopold, T. M. Miller, and W. C. Lineberger, J. Chem. Phys. **89**, 5442 (1988).
[198] R. L. Schwartz, G. E. Davico, T. M. Ramond, and W. C. Lineberger, J. Phys. Chem. A **103**, 8213 (1999).
[199] S. Koda, Chem. Phys. Lett. **55**, 353 (1978).
[200] S. Koda, J. Phys. Chem. **83**, 2065 (1979).
[201] S. Toby and F. S. Toby, J. Phys. Chem. **84**, 206 (1979).

[202] W.-Z. Chang, H.-J. Hsu, and B.-C. Chang, Chem. Phys. Lett. **413**, 25 (2005).
[203] M.-L. Liu, C.-L. Lee, A. Bezant, G. Tarczay, R. J. Clark, T. A. Miller, and B.-C. Chang, Phys. Chem. Chem. Phys. **5**, 1353 (2003).
[204] C. Kittrell, E. Abramson, J. L. Kinsey, S. McDonald, D. E. Reisner, D. Katayama, and R. W. Field, J. Chem. Phys. **75**, 2056 (1981).
[205] *Molecular Dynamics and Spectroscopy by Stimulated Emission Pumping* eds. H. L. Dai and R. W. Field (World Scientific, Singapore, 1995).
[206] B. Bohn and F. Stuhl, J. Chem. Phys. **102**, 8842 (1995).
[207] K. P. Huber and G. Herzberg, in *NIST Chemistry WebBook, NIST Standard Reference Database*, edited by P. J. Linstrom and W. G. Mallard (National Institute of Standards and Technology, Gaithersburg MD), Vol. 69.
[208] N. L. Owens, K. Nauta, S. H. Kable, N. L. Haworth, and G. B. Bacskay, Chem. Phys. Lett. **370**, 469 (2003).
[209] C. Tao, C. Richmond, C. Mukarakate, and S. A. Reid (unpublished) (2009).
[210] S. K. Shin and P. J. Dagdigian, J. Chem. Phys. **128**, 064309 (2008).
[211] G. P. Morley, P. Felder, and J. R. Huber, Chem. Phys. Lett. **219**, 195 (1994).
[212] G. B. Bacskay (unpublished) (2009).
[213] C. A. Richmond, J. S. Guss, K. Nauta, and S. H. Kable, J. Mol. Spectr. **220**, 137 (2003).
[214] Y. Kim, A. V. Komissarov, G. E. Hall, and T. J. Sears, J. Chem. Phys. **123**, 024306 (2005).
[215] E. J. Hintsa, X. Zhao, W. M. Jackson, W. B. Miller, A. M. Wodtke, and Y. T. Lee, J. Phys. Chem. **95**, 2799 (1991).
[216] B.-C. Chang, M. L. Costen, A. J. Marr, G. Ritchie, G. E. Hall, and T. J. Sears, J. Mol. Spectr. **202**, 131 (2000).
[217] A. J. Marr and T. J. Sears, J. Mol. Spectr. **195**, 367 (1999).